

Estimating precipitation on early Mars using a radiative-convective model of the atmosphere and comparison with inferred runoff from geomorphology

P. von Paris^{a,b,c,*}, A. Petau^a, J.L. Grenfell^a, E. Hauber^a, D. Breuer^a, R. Jaumann^a, H. Rauer^{a,d}, D. Tirsch^a

^a*Institut für Planetenforschung, Deutsches Zentrum für Luft- und Raumfahrt (DLR), Rutherfordstr. 2, 12489 Berlin, Germany*

^b*now at: Univ. Bordeaux, LAB, UMR 5804, F-33270, Floirac, France*

^c*now at: CNRS, LAB, UMR 5804, F-33270, Floirac, France*

^d*Zentrum für Astronomie und Astrophysik (ZAA), Technische Universität Berlin, Hardenbergstr. 36, 10623 Berlin, Germany*

Abstract

We compare estimates of atmospheric precipitation during the Martian Noachian-Hesperian boundary 3.8 Gyr ago as calculated in a radiative-convective column model of the atmosphere with runoff values estimated from a geomorphological analysis of dendritic valley network discharge rates. In the atmospheric model, we assume CO₂-H₂O-N₂ atmospheres with surface pressures varying from 20 mb to 3 bar with input solar luminosity reduced to 75% the modern value.

Results from the valley network analysis are of the order of a few mm d⁻¹ liquid water precipitation (1.5-10.6 mm d⁻¹, with a median of 3.1 mm d⁻¹). Atmospheric model results are much lower, from about 0.001-1 mm d⁻¹ of snowfall (depending on CO₂ partial pressure). Hence, the atmospheric model predicts a significantly lower amount of precipitated water than estimated from the geomorphological analysis. Furthermore, global mean surface temperatures are below freezing, i.e. runoff is most likely not directly linked to precipitation. Therefore, our results strongly favor a cold early Mars with episodic snowmelt as a source for runoff.

Our approach is challenged by mostly unconstrained parameters, e.g. greenhouse gas abundance, global meteorology (for example, clouds) and planetary parameters such as obliquity- which affect the atmospheric result - as well as by inherent problems in estimating discharge and runoff on ancient Mars, such as a lack of knowledge on infiltration and evaporation rates and on flooding timescales, which affect the geomorphological data. Nevertheless, our work represents a first step in combining and interpreting quantitative tools applied in early Mars atmospheric and geomorphological studies.

Keywords:

early Mars: habitability, precipitation, atmospheres, geomorphology

*Corresponding author: email vonparis@obs.u-bordeaux1.fr, tel. +33 (0)557 77 6131

1. Introduction

Habitability defined as the conditions suitable for life (e.g., Mars Exploration Program Analysis Group 2005) has become a central concept in both Solar System and exoplanet science. Early Mars is arguably the key environment to study whether habitable conditions could arise away from the Earth.

In this work we apply an atmospheric model to estimate global mean precipitation rates on early Mars. These are then compared with runoff rates as derived from a geomorphological data analysis of a sample of valley networks. Our main aim is not to investigate the formation of individual networks. Rather, we aim to assess (i) the probable strength of the overall hydrological cycle on early Mars in terms of the amount of precipitated water needed to form the networks, and (ii) whether the atmospheric conditions would have allowed for such a hydrological cycle, again in terms of amount of precipitated water, but also in terms of temperature (snow vs. rainfall).

We begin (Section 1.1) by discussing processes affecting atmospheric formation and composition since these are critical for the early Mars climate hence habitability. Then we give an overview of the geomorphological valley features (Section 1.2) observed on Mars which provide key evidence that early Mars was wet. Section 2 presents the tools used and their constraints. Section 3 presents results, comparing precipitation rates from the atmospheric model with those from the geomorphological approach. Section 4 presents a discussion and Section 5 shows conclusions.

1.1. Background on early Mars Atmosphere

Constraints on atmospheric composition and mass for the early Martian atmosphere can be obtained from a combination of outgassing and escape modeling as well as measurements of e.g. isotopic ratios of nitrogen, oxygen and carbon. Degassing during the early magma ocean phase could have led to an atmosphere of tens of bars or more, but this was probably efficiently removed very fast either during the magma-ocean phase or at the latest during the first few hundred million years due to strong solar activity (e.g., Tian et al. 2009, Lammer et al. 2013). Later input by outgassing is likely insufficient to form dense CO₂ atmospheres of the order of a few bars. Model studies suggest a maximum of about 0.5-1.5 bar before 3.8 Gyrs (e.g., Phillips et al. 2001, Grott et al. 2011), with the lower value being more realistic considering the low oxygen fugacity of the Martian mantle and that crustal recycling was inefficient in Mars (e.g., Stanley et al. 2011). However, impacts during the late heavy bombardment may have provided additional atmospheric mass (up to a few bars, e.g., de Niem et al. 2012). Isotopic ratios (e.g., Jakosky and Phillips 2001, Fox and Hać 2010, Gillmann et al. 2011) and an in-situ analysis of estimated rock trajectories during explosive volcanic eruptions (e.g., Manga et al. 2012) also suggest a denser atmosphere than today. Upper limits on early Mars atmospheric pressure of about 1 bar have been reported recently based on crater analysis (Kite et al. 2014). A key challenge is how to remove considerable amounts of atmosphere in order to arrive at the present, thin atmosphere, since loss processes are not thought to be efficient after the Noachian period (e.g., Lammer et al. 2013).

The early Mars atmosphere is thought to be composed mainly of CO₂, as suggested by outgassing models (e.g., Phillips et al. 2001), although such studies also predict significant H₂O outgassing (e.g., Grott et al. 2011). Trace gases could have been present in the atmosphere, e.g. SO₂ due to volcanic outgassing (e.g., Farquhar et al. 2000, Halevy et al. 2007) or O₃ due to atmospheric photochemistry (e.g., Selsis et al. 2002). Atmospheric N₂ may have been present since its original inventory is relatively large (e.g., McKay and Stoker 1989). Other radiatively active gases such as CH₄ have also been suggested (e.g., Postawko and Kuhn 1986). Recent studies investigated the possibility of H₂-induced warming (e.g., Ramirez et al. 2014) because H₂ could have been a major atmospheric constituent due to enhanced outgassing from the reduced early Mars mantle. However, most atmospheric model studies only investigated CO₂-H₂O scenarios, some with the addition of either SO₂, H₂ or N₂, but currently no model has used a combination of all of these gases.

Early 1D CO₂-H₂O atmospheric model studies by, e.g., Kasting (1991) suggested mean surface temperatures far below freezing, indicating that sustained rainfall might not be the reason for producing observed fluvial features. One possible mechanism suggested for warming early Mars includes the formation of CO₂ clouds (e.g., Pierrehumbert and Erlick 1998, Forget and Pierrehumbert 1997). However, 1D and 3D modeling studies suggested that the cloud cover would have to be nearly 100% (e.g., Mischna et al. 2000), which is unrealistic as found by more detailed, time-dependent 1D or 3D simulations (e.g., Colaprete and Toon 2003, Wordsworth et al. 2013). Recent radiative transfer modeling studies (Kitzmann et al. 2013) suggested that the overall warming effect might have been strongly overestimated.

Most recent 1D atmospheric modeling studies continue to calculate mean surface temperatures below freezing even when including the presence of additional greenhouse gases such as SO₂ (e.g., Tian et al. 2010) or N₂ (e.g., von Paris et al. 2013a). In contrast, the new study by Ramirez et al. (2014) found mean surface temperatures well above freezing upon simulating dense CO₂-H₂ atmospheres. Kahre et al. (2013) speculate that a highly active dust cycle on early Mars could have warmed the surface. Dust could have warmed the surface by up to 10 K depending on dust opacity (Forget et al. 2013). A reduction in surface albedo (e.g. due to a larger exposure of basaltic bedrock) has been suggested to warm the surface by, e.g., Fairén et al. (2012) and Mischna et al. (2013).

With 3D model studies (e.g., Johnson et al. 2008, Wordsworth et al. 2013, Mischna et al. 2013, Urata and Toon 2013), the problem of cold global mean surface temperatures could be addressed to some extent: They showed that even for mean surface temperatures below freezing, large areas of the Martian surface could remain much warmer, with annual means of 260-270 K. In addition, 3D global and mesoscale models of the early Mars climate suggest that orography could be an important factor to drive precipitation. In a recent study, Scanlon et al. (2013) show that orography-driven precipitation in the form of snowfall (of the order of about 10⁻²-10⁻¹ kg d⁻¹ m⁻²) coincides roughly with the location of former rivers on early Mars.

1.2. Background on Geomorphology: Martian Valley Networks

The term valley networks denotes fluid-carved systems of incisions on planetary surfaces, interpreted to be former river valleys. Less degraded fluvial valleys may

still possess a narrow interior channel along the valley bottom, which represents the riverbed itself (e.g., Jaumann et al. 2005). Valley networks on Mars occur in two generic types, namely "dendritic" and "longitudinal". Each type implies a different hydrological regime. Dendritic patterns are interpreted to be indicative of precipitation-fed surface runoff due to their analogy to terrestrial features (e.g., Craddock and Howard 2002, Irwin et al. 2005, Barnhart et al. 2009, Ansan and Mangold 2013). The surface runoff can be either caused by snowmelt or rain whereby recent studies emphasize that episodic snowmelt might be the most favorable process of water release (e.g., Forget et al. 2013, Wordsworth et al. 2013, Scanlon et al. 2013). Longitudinal valleys may represent fluvial channels, but featuring only a few tributaries.

Whereas some authors propose erosion by groundwater seepage (sapping) as the most plausible water release mechanism for these channels (e.g., Malin and Carr 1999, Goldspiel and Squyres 2000, Harrison and Grimm 2005, Jaumann et al. 2010), others have demonstrated that sapping alone does not account for the erosion at analogous terrestrial channels and a significant contribution by overland runoff is required (e.g., Lamb et al. 2008). Valley networks on Mars occur mostly in the heavily cratered southern highlands whereas some isolated fluvial channels have been observed along the flanks of volcanic edifices (e.g., Gulick and Baker 1990, Carr 1995, Fassett and Head 2006, Hynes et al. 2010).

Crater size-frequency analyses of valley network-incised regions show that fluvial activity peaks during the late Noachian and sharply decreases after the early Hesperian (e.g., Fassett and Head 2008, 2011, Hoke and Hynes 2009). Nevertheless, recent research has shown that aqueous surface processes continued even after the early Hesperian, though on a less intense level (e.g., Fassett et al. 2010, Howard and Moore 2011, Hauber et al. 2013, Parsons et al. 2013, Hobley et al. 2014). A recent study by Buhler et al. (2014) suggests intermittent (not continuous) fluvial activity of the order of 10^{-3} of the available time to form the networks, based on complex transport and hydrological analyses.

2. Tools and Methods

2.1. Atmosphere

We use atmospheric profiles of pressure p , temperature T and water concentrations $c_{\text{H}_2\text{O}}$ from calculations presented in von Paris et al. (2013a). These profiles were obtained with a 1D steady-state, radiative-convective atmospheric model which simulates globally averaged conditions. The model solves the radiative transfer equation and accounts for convective energy transport in the lower atmosphere by performing instantaneous convective adjustment to the (wet) adiabatic lapse rate. Further details can be found in von Paris et al. (2013a) and references therein. Model atmospheres were assumed to be composed of varying amounts of CO_2 (8 values between 0.02-3 bar) and N_2 (5 values between 0-0.5 bar). Solar irradiation was set to be consistent with Noachian conditions 3.8 billion years ago, i.e. 75 % of today's irradiation (e.g., Gough 1981).

Figure 1 shows the calculated surface temperatures (black lines) and planetary albedos (red lines). The planetary albedo increases due to enhanced Rayleigh scattering

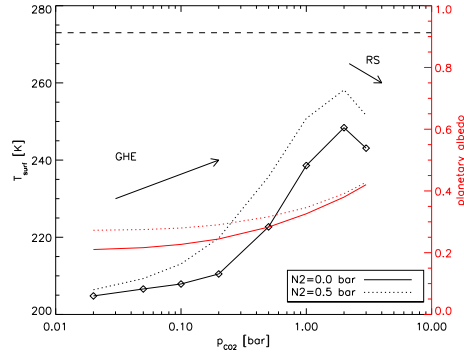


Figure 1: Surface temperatures (black) and planetary albedo (red) as a function of CO₂ partial pressure at two values of N₂ partial pressure (plain: 0 bar, dotted: 0.5 bar), values taken from simulations of von Paris et al. (2013a). 273 K indicated by horizontal dashed line. RS=Rayleigh scattering (cooling), GHE=Greenhouse effect (warming).

which scales with atmospheric mass, hence also the higher albedo in the 0.5 bar N₂ case. With increasing CO₂ partial pressures, both the zero N₂ case (plain line) and the 0.5 bar N₂ case (dotted line) approximately converge to the same albedo since CO₂ is a much more efficient scatterer than N₂ (Vardavas and Carver 1984) and dominates the scattering optical depth. Surface temperatures show a distinct maximum. This is because the surface temperature first increases when increasing CO₂ due to an enhanced greenhouse effect, reaching 248 K at 2 bar of CO₂ and zero N₂. Adding 0.5 bar of N₂ increases the surface temperature by up to 12 K, depending on CO₂ partial pressure. Above (2-3) bars of surface CO₂, the greenhouse effect saturates. An opposing, cooling effect via the strong Rayleigh scattering becomes important, and surface temperatures decrease again. This effect is known as the maximum greenhouse effect (e.g., Kasting 1991, Kasting et al. 1993, Tian et al. 2010, von Paris et al. 2013a).

Water concentration profiles as a function of altitude z in von Paris et al. (2013a) were calculated from the following equation:

$$c_{\text{H}_2\text{O}}(z) = \text{RH}(z) \cdot \frac{p_{\text{sat,H}_2\text{O}}(T(z))}{p(z)} \quad (1)$$

where RH is the Relative Humidity and $p_{\text{sat,H}_2\text{O}}(T(z))$ the temperature-dependent water saturation vapour pressure. RH is thus defined as the water vapour pressure relative to the saturation vapour pressure and is a measure of the amount of water able to be held in the gas-phase. It depends on e.g. T-p conditions, and (sensitively) to the heterogenous surface loading (dust, aerosol) of the atmosphere (which is not known for early Mars). RH is therefore not well constrained in the early Martian atmosphere. Previous 1D studies usually assumed either a fully-saturated troposphere, i.e. RH=1, or 50 % saturation, i.e. RH=0.5 (e.g., Mischna et al. 2000, Colaprete and Toon 2003, Tian et al. 2010). The calculations in von Paris et al. (2013a) also used RH=1. For 1D simulations of modern Earth or hypothetical terrestrial exoplanets, the RH profile is often based on the observed mean Earth profile of Manabe and Wetherald (1967)

(RH=MW, e.g., Segura et al. 2003, Grenfell et al. 2007, Wordsworth et al. 2010b).

From the calculated water profiles of Eq. 1, it is possible to obtain the mean atmospheric water column ($C_{\text{H}_2\text{O}}$ in units of kg m^{-2} , see Figure 3 in von Paris et al. 2013a), via:

$$C_{\text{H}_2\text{O}} = \frac{m_{\text{H}_2\text{O}}}{g\mu} \cdot \sum_{i=1}^{N-1} c_{\text{H}_2\text{O},i}(p_i - p_{i+1}) \quad (2)$$

where N is the number of atmospheric levels (here, $N=52$, $i=1$ at surface), g the planetary gravity (for Mars, $g=3.73 \text{ m s}^{-2}$), μ the mean atmospheric weight, $m_{\text{H}_2\text{O}}$ the molecular weight of water and $c_{\text{H}_2\text{O},i}$, p_i water concentrations and pressure in level i .

In atmospheric 1D and 3D models, precipitation is calculated, e.g., by assigning precipitation efficiencies to cloud layers (e.g., Rennó et al. 1994), choosing a precipitation threshold for the water content (e.g., Wordsworth et al. 2013) or simply assuming that clouds at the surface precipitate all super-saturated water (e.g., Segura et al. 2008). In this work, we choose a different approach, as follows. The mean precipitation on Earth is $\approx 2.6 \text{ mm d}^{-1}$, i.e. $2.6 \text{ kg m}^{-2} \text{ d}^{-1}$ (e.g., Xie and Arkin 1997, Mitchell and Jones 2005, Adler et al. 2012). Taking a mean Earth water column of $C_{\text{H}_2\text{O,Earth}}=19.5 \text{ kg m}^{-2}$ (see e.g., modern Earth atmospheric simulations by Grenfell et al. 2007), this amounts to a daily precipitation rate, $pr=13.3\%$ of the total water column. In this work we apply this value of pr (which is clearly a source of uncertainty, see discussion below) to the early Mars scenarios (see Fig. 1) to calculate precipitation rates P :

$$P = pr \cdot C_{\text{H}_2\text{O}} \quad (3)$$

For example, von Paris et al. (2013a) found, at a CO_2 partial pressure of 2 bar and 0.5 bar of N_2 , a water column of 5.2 kg m^{-2} (see their Fig. 3). The corresponding mean precipitation would then be 0.7 mm d^{-1} , i.e. around 26% of the mean Earth value.

To explore uncertainties in this simple, first-order approach, we perform the following sensitivity studies regarding three important parameters for the calculation of precipitation, i.e. the assumed percentage precipitation pr , the RH profile and the surface temperature:

Atmospheric Precipitation

We vary pr in Eq. 3 assumed for early Mars as follows. On Earth (mean $pr=13.3\%$), there is a latitudinal gradient in pr , due to global circulation and the land-ocean distribution. Figure 2 shows the latitudinal gradient of the annual means of water column and precipitation. The values are based on monthly averages for the year 2013, accessed through the NCEP/NCAR (Kalnay et al. 1996) website <http://www.esrl.noaa.gov/psd/cgi-bin/data/timeseries/timeseries1>. Figure 3 then shows the associated value of pr , using eq. 3. For the most part (except south polar regions, where water column measurements are very uncertain), pr remains between about 8-30%. Hence, we varied pr based on the extremes found on modern Earth, i.e. $pr=8, 13.3$ and 30% . Idealized 3D simulations by O’Gorman and Schneider (2008) found that the atmospheric water residence time $\tau_w = 1/pr$ depends on surface temperature and actually increases for warmer climates, broadly consistent with modern Earth observations (see Fig. 3). The actual amount of precipitation depends on the

amount of available water in the atmospheric column as well as the precipitation efficiency pr , which can both be calculated consistently in a 3D model. However, in this work, we only calculate the water column as a function of atmospheric composition and vary pr within a reasonable range.

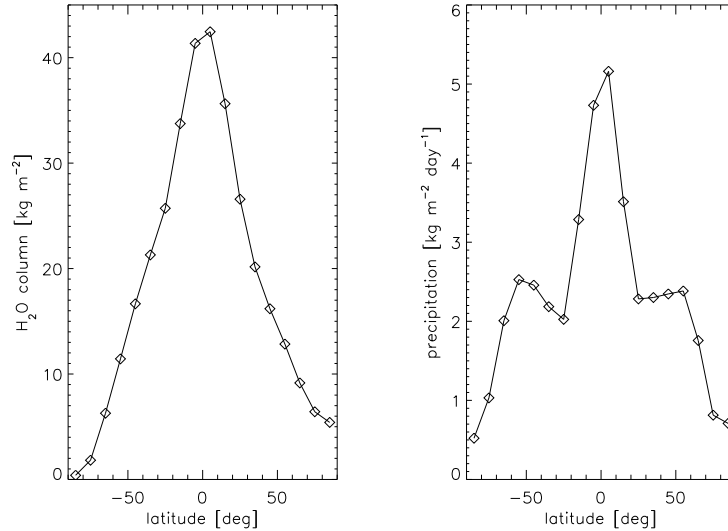


Figure 2: Latitudinal gradient of water column (left panel) and precipitation (right panel). 10° -averaged annual mean for year 2013, based on the NCEP/NCAR project (Kalnay et al. 1996). Data set available through <http://www.esrl.noaa.gov/psd/cgi-bin/data/timeseries/timeseries1.pl>

How accurate is this approach? Using 3D GCM simulations of early Mars presented by Wordsworth et al. (2013), we estimated their pr value to be of the order of 20-50% (their Fig. 10 and Table 2), comparable to polar values on Earth (see Fig. 3). This estimate of pr is obtained as follows: On summing (by eye) the panels describing seasonal snowfall in Fig. 10 of Wordsworth et al. (2013) and using their stated water column of the 1 bar simulation (0.07 kg m^{-2} , see their Table 2), we found a range for pr of 20-50%. On early Mars, clearly several factors such as the Martian dichotomy will influence global convection, hence the strength of the Hadley cell. Nevertheless these factors are not well defined so our assumption based on the Earth is a reasonable first estimate.

Atmospheric Relative Humidity

To investigate uncertainties in early Mars' RH profiles (see above), we introduced two new RH test cases, namely (i) $\text{RH}=0.5$ and (ii) $\text{RH}=\text{MW}$, in addition to the original $\text{RH}=1$ from von Paris et al. (2013a). These three profiles are shown in Fig. 4. Note that although the MW profile drops sharply with altitude, within the lowermost atmospheric scale height ($\frac{p}{p_{\text{surf}}} = 0.36$, indicated by horizontal line) where most of the water resides, the three RH profiles are rather similar.

We repeated the zero- N_2 simulations with the atmospheric model of von Paris et al. (2013a), using the new RH profiles (i.e., $\text{RH}=0.5$ and $\text{RH}=\text{MW}$). The effect on sur-

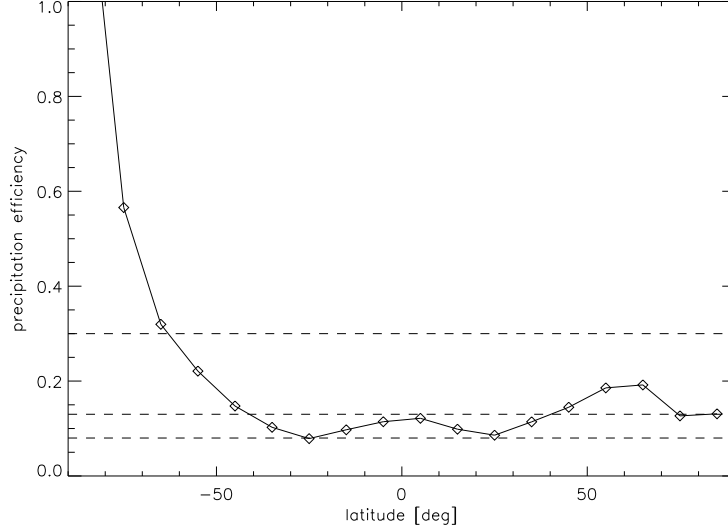


Figure 3: Latitudinal gradient of precipitation rate pr , based on Fig. 2.

face temperature was on the order of a few K, comparable to 1D results obtained by Colaprete and Toon (2003). Note that 3D simulations performed by Wordsworth et al. (2013) find a somewhat larger effect of up to 20 K. Water columns decreased by about 30-50 % when compared to the RH=1 case, as shown in Fig. 5.

Surface temperature

Here, we estimated the effect of a (local) surface temperature increase ΔT (with respect to the zero N_2 scenarios) upon precipitation (see Fig. 12 and discussion there). The surface temperature and the temperature profile are very important factors when calculating precipitation rates because the water vapour saturation pressure $p_{\text{sat,H}_2\text{O}}$, hence the water concentration profile (see Eq. 1), depend strongly on temperature. We add ΔT to both the surface temperature and the temperature profile from von Paris et al. (2013a). The water profile and the resulting column are then re-calculated with Eqs. 1 and 2. This simplifying approach is justified since most of the water column resides near the surface where the temperature lapse rate is approximately constant with altitude, at about $3\text{-}4 \text{ K km}^{-1}$, which is close to the dry adiabatic value of 4.3 K km^{-1} .

Global mean vs local precipitation

There exists not only a latitudinal gradient in mean precipitation (Fig. 2), but also a monthly variation, as shown in Fig. 6. Therefore, at any given location and given time, the actual local precipitation P_{loc} might not be well represented by the global mean precipitation P_{glob} . Rather, in an extremely simplified approach, one might relate these through

$$P_{\text{loc}} = x \cdot P_{\text{glob}} \quad (4)$$

where x must be determined by temporally and spatially resolved calculations.

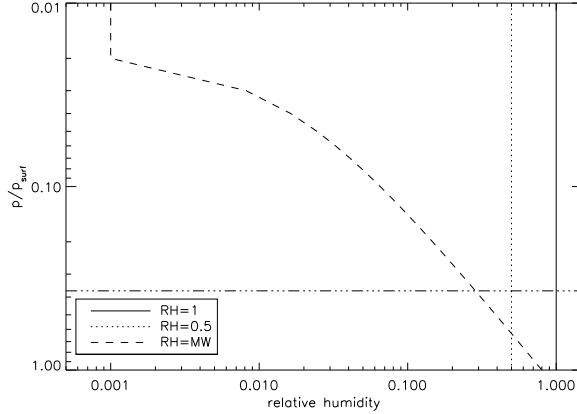


Figure 4: Relative humidity profiles used in this work. Lowermost atmospheric scale height indicated by horizontal triple-dot-dashed line.

However, as indicated by Figs. 2 and 6, on spatial scales resolved by present-day 3D GCM simulations, x is probably not larger than about 3. Mesoscale 3D models of early Mars have shown that orography-driven precipitation can be much stronger (up to an order of magnitude) than synoptic-scale precipitation (Scanlon et al. 2013), suggesting values of up to $x=10$ for increasingly finer spatial resolutions.

In a last parameter variation, we therefore estimated an approximate value for x in order to obtain an agreement between atmospheric model and geomorphology data.

2.2. Geological Constraints

2.2.1. Methods

Most valley networks represent relics of ancient fluvial activity on early Mars near the Noachian-Hesperian boundary. Thus, it is not possible to measure directly discharge rates Q (in units of m^3s^{-1}). They are instead derived from parameters related to the valley system's morphometric properties, channel width W_C , depth D , and the flow velocity v :

$$Q = W_C \cdot D \cdot v \quad (5)$$

The depth D of the Martian riverbed is usually not available. It is in most cases too small to be resolved in the Digital Terrain Models (DTM) derived from, e.g. Mars Express's HRSC (High Resolution Stereo Camera, Jaumann et al. 2007, Gwinner et al. 2010) and Mars Global Surveyor's MOLA (Mars Orbiter Laser Altimeter, Smith et al. 2001). Furthermore, the flow velocity v is also unknown. Therefore, Q can only be derived based on the channel width W_C , which is in principle observable. The lack of reliable information on the stability of the channel banks complicates accurate measurements of W_C . However, empirical correlations can be used to estimate discharge rates from the width of the channels. On Earth, for channels in the Missouri river area,

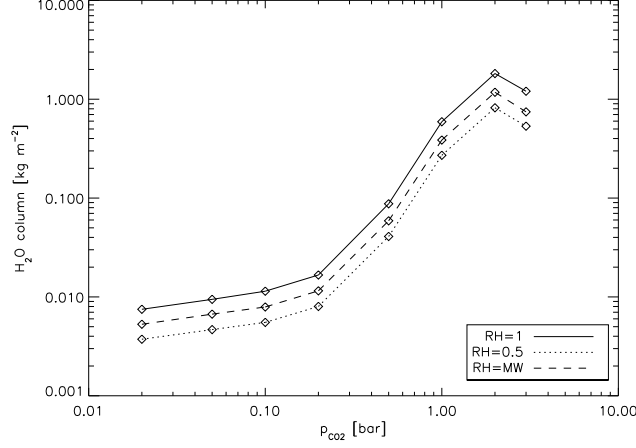


Figure 5: H₂O column as a function of CO₂ pressure: Influence of relative humidity profiles. Zero N₂.

Osterkamp and Hedman (1982) use an empirical power law equation ($Q = f \cdot W_C^e$) to obtain mean discharge rates:

$$Q_{\text{Earth,mean}} = f_{\text{Earth}} \cdot W_C^{e_{\text{Earth}}} = 0.027 \cdot W_C^{1.71} \quad (6)$$

The main assumption in this work and others (e.g., Irwin et al. 2005) is that Q scales with the same power law, meaning the exponent e_{Earth} does not change for Martian channels (i.e., $e_{\text{Earth}} = e_{\text{Mars}}$). Only the scaling factor f_{Mars} will be adjusted to Martian gravity based on the value of f_{Earth} . To obtain a conservative estimate of the channel width, we follow the approach of Irwin et al. (2005). We use narrow, straight channel sections to measure channel widths. It is assumed that channel bank-to-bank widths are less modified in such areas. Thus, this approach helps minimizing the impact of subsequent mass movements that could heavily modify channel bank-to-bank widths.

To calculate f_{Mars} , we follow the approach of Irwin et al. (2005) and Moore et al. (2003). They assumed that the channel width W scales with relative gravity g ($=0.38$ for Mars/Earth system) as $g^{-0.23}$. For the same unit discharge Q , since $e_{\text{Earth}} = e_{\text{Mars}}$, we have then:

$$f_{\text{Mars}} = f_{\text{Earth}} \left(\left(\frac{g_{\text{Mars}}}{g_{\text{Earth}}} \right)^{-0.23} \right)^{-e_{\text{Mars}}} = 0.018 \quad (7)$$

Inserting into eq. 6 leads to the following empirical relation between W and Q on Mars

$$Q_{\text{Mars,mean}} = 0.018 W_C^{1.71} \quad (8)$$

Local variations of W by later erosion and modification processes result in a possible error of a factor of 2; a further factor of 3 may arise via the unknown stability of the banks and is also inherent in the empirical equation itself (Irwin et al. 2005). Thus,

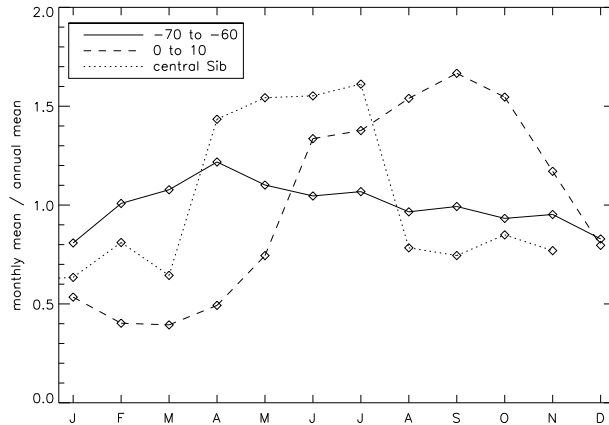


Figure 6: Variation of the monthly mean precipitation around the annual mean for different locations on Earth (zonal means at given latitude and in Central Siberia). Data set available through <http://www.esrl.noaa.gov/psd/cgi-bin/data/timeseries/timeseries1.pl>

the results for Q are conservative estimates, but are most likely accurate to within an order of magnitude. Once the discharges have been derived, the runoff rate R can then be estimated:

$$R = \frac{Q}{C} \quad (9)$$

where Q is the discharge rate of a valley network at its outlet and C the respective catchment area. This results in a water equivalent layer from a few millimeters up to several centimeters thick per d.

2.2.2. Data set

In total, we used runoff values of 18 valley networks in our analysis, as presented in Table 1. Their distribution is indicated in Fig. 7. It is generally accepted that surface runoff occurred mainly at the transition between Noachian/Hesperian 3.7-3.8 billion years ago and earlier (e.g., Fassett and Head 2008, Hynes et al. 2010). At this time, there was a major decrease in runoff intensity on the Martian surface (Carr and Head 2010). Hence the data set is assumed to be consistent in time with the atmospheric model simulations.

Their channel widths and the corresponding discharge rates have been determined. Where available, direct measurements of W_C have been used to calculate Q via Eq. 8. However, most of these valleys do not show any channels (because they are completely covered with sediment or destroyed by erosion). Hence, channel widths W_C for Eq. 8 have been deduced from the measured valley width W_V via a simple scaling suggested by Penido et al. (2013):

$$W_C = 0.14 \cdot W_V \quad (10)$$

Table 1: Valley networks used in this work (measured quantities in bold).

Identifier	location	W_V [m]	W_C [m]	C [km ²]	Q_{mean} [m ³ s ⁻¹]	R_{mean} [mm d ⁻¹]	Q_{peak} [m ³ s ⁻¹]	R_{peak} [mm d ⁻¹]
8604-1	38°15' S/ 203° E	-	250	1840	226.8	10.65	1179.2	55.3
8604-2	38°27' S/ 204° E	-	220	2970	182.3	5.30	1008.9	29.3
8604-3	38°30' S/ 204°5' E	-	255	2230	234.6	9.09	1208.1	46.8
H1226_0000_ND3	1°52' N/ 89°25' E	1770	247	12840	222.2	1.49	1162.0	7.8
H5212_0000_ND3	1°49' N/ 121°16' E	5850	819	21240	1725.7	7.02	5015.7	20.4
H2081_0000_ND3	0°15' N/ 124°12' E	2070	289	4240	290.6	5.92	1407.4	28.6
H0430_0000_ND3	36°57' S/ 7°56' E	480	67	300	23.8	6.87	236.5	68.1
H2181_0001_ND3	45°29' S/ 17°16' E	1430	200	3030	154.8	4.41	898.2	25.6
H5168_0001_ND3-2	10°47' S/ 156°45' W	1180	165	3530	111.4	2.72	710.3	17.3
H2689_0001_ND3	34°40' S/ 146°04' E	2120	296	9070	302.8	2.88	1449.1	13.8
H7213_0000_ND3	12°21' S/ 177°58' W	2040	285	14120	283.8	1.73	1383.6	8.4
H2459_0009_ND3	17°6' S/ 65°42' E	2790	390	15950	485.2	2.62	2028.7	10.9
H2347_0000_ND3	52°49' S/ 90°49' W	1880	263	8400	247.3	2.54	1254.5	12.9
H2475_0000_ND3-1	49°19' S/ 65°28' W	-	160	6040	105.7	1.51	684.1	9.7
H2475_0000_ND3-3	52°26' S/ 65°51' W	1030	144	2430	88.3	3.14	601.6	21.3
H4290_0000_ND3	35°3' S/ 132° E	-	270	7170	258.7	3.11	1295.3	15.6
H2539_0000_ND3	27°16' S/ 128°10' E	1600	224	1720	188.0	9.44	1031.4	51.8
H6438_0000_ND3	24°54' S/ 3°26' W	2880	403	18230	513.2	2.43	2111.5	10.0

Table 2: Comparison of peak discharge and runoff rates.

Region/name	Q_{peak} [m ³ s ⁻¹]	R_{peak} [cm d ⁻¹]	references
global distribution (see Fig. 7)	236-5015	0.8-6.8	this work
global distribution	300-5800	0.1-6	Irwin et al. (2005)
Terra Sabaea, Arabia Terra, Meridiani Plan.	7,000-70,000	0.4-63	Hoke et al. (2011)

Subsequently, the sizes of the respective catchment areas C were determined using topographic data based by HRSC and MOLA DTMs (e.g., Gwinner et al. 2010, Smith et al. 2001).

The runoff rates were calculated from Eq. 9, resulting in a mean runoff of 1.5-10.65 mm d⁻¹, depending on valley location. The median value of our dataset is 3.14 mm d⁻¹, relatively close to the mean Earth precipitation of 2.6 mm d⁻¹. As is apparent from Fig. 2 and Table 1, quite a few valley networks require precipitation rates close to or higher than typical tropical values found on Earth. Overall, therefore, these runoff rates would suggest a very strong, global mean hydrological cycle on early Mars, if the networks indeed formed throughout extended periods of warm climate.

2.2.3. Comparison with previous work

To compare the runoff rates for our networks with rates previously published in the literature, we need to calculate peak instead of mean runoff rates (also shown in Table 1). Note that when comparing to a global mean atmospheric model, as is the aim in

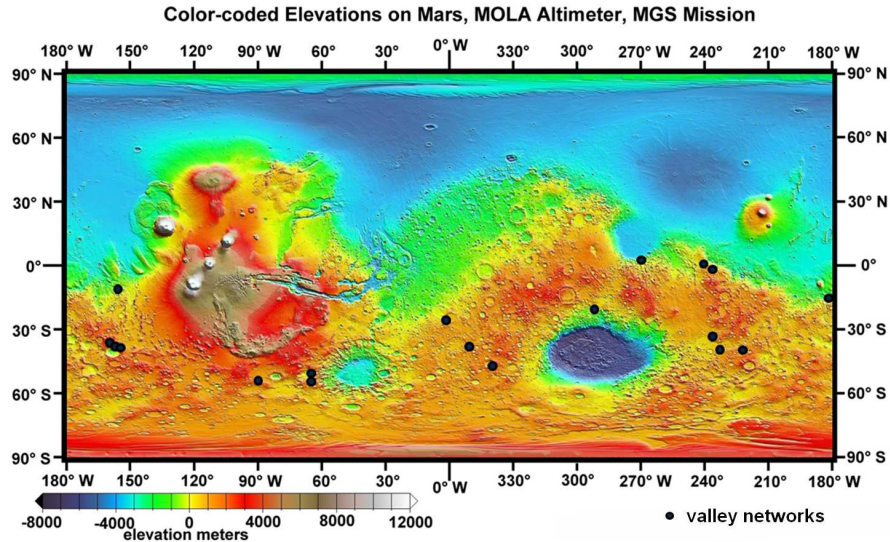


Figure 7: Distribution of the 18 valley networks (black dots) used in this work.

this work, we should use mean runoff rates. In a similar reasoning as for deriving eq. 8, based on the peak discharge approximation from Osterkamp and Hedman (1982) we obtain

$$Q_{\text{Mars,peak}} = 1.4W_C^{1.22} \quad (11)$$

Peak runoff rates from our 18 valley networks are between 0.8 cm d^{-1} and 6.8 cm d^{-1} . Irwin et al. (2005) find runoff rates of 0.1 cm d^{-1} to 6 cm d^{-1} . In contrast to our study, Hoke et al. (2011) investigated larger valley systems, which results in runoff rates of 0.4 cm d^{-1} to 63 cm d^{-1} . In general, our results are in good agreement with the measurements of other investigations of Martian peak runoff rates (see Table 2). In a very recent work, Palucis et al. (2014) estimated discharge (not runoff) from a channel in Gale Crater (average channel width 27 m). They found values ranging from $3.7\text{-}6.5 \text{ m}^3 \text{ s}^{-1}$ when assuming a shallow channel and up to $117\text{-}207 \text{ m}^3 \text{ s}^{-1}$ for deeper channels. This compares reasonably well to estimates from our simple equations 8 ($5 \text{ m}^3 \text{ s}^{-1}$) and 11 ($78 \text{ m}^3 \text{ s}^{-1}$) when using the stated channel width of 27 m.

3. Results

Figure 8 shows our precipitation rates as a function of CO_2 partial pressure as inferred from the atmospheric model for the scenarios discussed. Also shown are derived mean runoff rates (horizontal lines) from valley network data (minimum, median and maximum). We show atmospheric scenarios with zero and 0.5 bar N_2 . The atmospheric model results display a maximum in precipitation rate, as could be expected from Fig. 1.

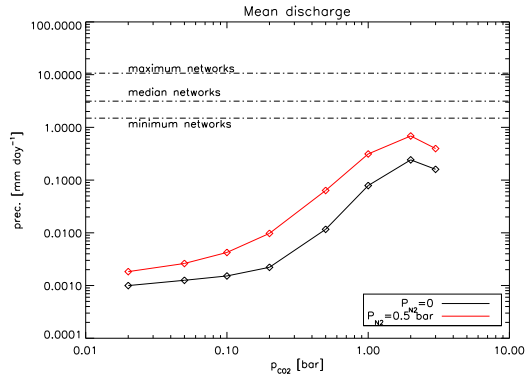


Figure 8: Total precipitation (mm d^{-1}) versus surface CO_2 pressure output from the atmospheric column model (von Paris et al. 2013a, $\text{RH}=1$) assuming $pr=13.3\%$. Black: No N_2 , red: 0.5 bar N_2 . Mean discharge from Eq. 8.

Figure 8 suggests that the calculated mean precipitation rates are lower by more than an order of magnitude compared to the median mean runoff value derived from the network data. Even the minimum runoff from the valley networks still is roughly 7 times higher than the maximum value calculated from the zero N_2 case.

Figure 9 shows the effect of adopting different relative humidity profiles on the calculated precipitation rate. As expected, since most of the water column lies in the lowermost atmospheric layers, the effect is rather small, even when reducing the RH from $\text{RH}=1$ to the MW RH profile, although it amounts to roughly a factor of 2 decrease compared to the fully saturated $\text{RH}=1$ case.

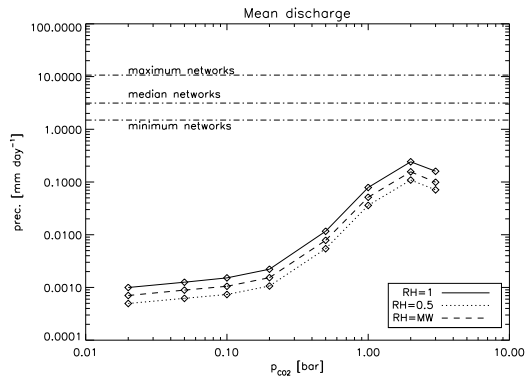


Figure 9: Total precipitation (mm d^{-1}) versus surface CO_2 pressure output from the atmospheric column model (von Paris et al. 2013a, zero N_2 , $pr=13.3\%$). Effect of varying RH. Plain line: $\text{RH}=1$, dotted: $\text{RH}=0.5$, dashed: $\text{RH}=\text{MW}$.

Figure 10 shows the influence of varying the adopted pr value on precipitation rates. For the lower (Earth) values of $pr = 8\%$ the disagreement between atmospheric and geological data becomes stronger, as expected, i.e. a significant additional dis-

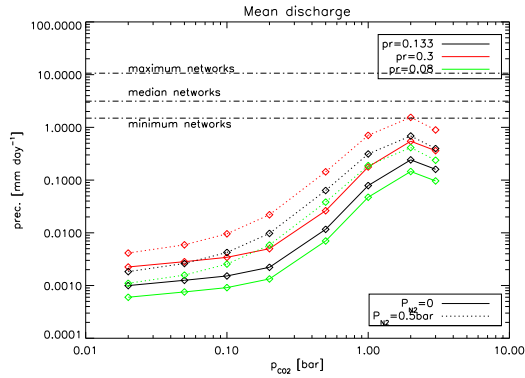


Figure 10: Total precipitation (mm d^{-1}) versus surface CO_2 pressure output from the atmospheric column model (von Paris et al. 2013a, $\text{RH}=1$, plain: zero N_2 , dotted: 0.5 bar N_2). Effect of varying percentage precipitation. Black: $pr=13.3\%$, red: $pr=30\%$, green: $pr=8\%$.

agreement of a factor of about three between atmospheric and geological data becomes apparent. Only in the most favorable case (high N_2 , high pr) can the atmospheric model reproduce roughly the lowest precipitation value inferred from the valley networks.

Figure 11 shows our favored estimates of early Mars precipitation, with $\text{RH}=\text{MW}$ and $pr=0.3$. The use of $\text{RH}=1$ was justified by the absence of any realistic information on the relative humidity distribution on early Mars. Results by Wordsworth et al. (2013) suggest that the atmosphere was most likely significantly drier, therefore we choose $\text{RH}=0.5$ which yields our driest runs (see Fig. 5). The favored estimate of early Mars precipitation is 0.3, which is closer to Earth polar values (see Fig. 3) and estimates from Wordsworth et al. (2013). We also show precipitation estimates with $x=10$ (taken from Scanlon et al. 2013, see eq. 4).

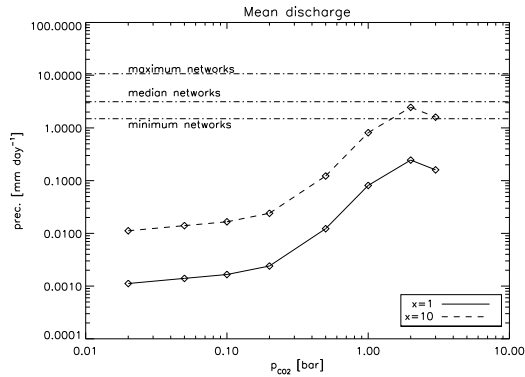


Figure 11: Most favored estimates of precipitation: $\text{RH}=0.5$, $pr=0.3$, for different values of x .

It is clearly seen that in this case, the disagreement between global mean atmospheric and valley network data remains substantial. However, for large values of x ,

estimated amounts of precipitated water become somewhat closer to each other. Still, it is unclear which mechanisms would drive x to the needed values of $x > 10-20$ (or even higher at lower CO_2 pressures). This remains a question for future work.

4. Discussion

4.1. Runoff from rain or snowmelt?

The aim of this work has been to compare precipitation rates calculated with a 1D atmospheric model to runoff rates inferred from geomorphological data. For this comparison to be meaningful, one critical condition must be fulfilled, i.e. precipitation P is the source for runoff Q .

As is apparent from Fig. 1, calculated global mean surface temperatures are far below freezing, hence P would mainly occur as snowfall than as rain (Wordsworth et al. 2013) and therefore would not be linked directly to Q . Numerous studies suggest a possibly significant contribution by snowmelt (e.g., Clow 1987, Kite et al. 2013, Wordsworth et al. 2013, Palucis et al. 2014), when orbital elements are suitable. Hence, snowmelt rather than precipitation may have been the dominant factor in producing liquid water available for runoff. Snow melt is a highly time-dependent process, and will concentrate discharge in river channels over short periods of time in spring and early summer (or whenever orbital elements favor local melt conditions), whereas discharge is much lower in the rest of the year (e.g., Bavay et al. 2009). On Earth, runoff over the majority of the land area in the northern hemisphere is seasonally variable (Weingartner et al. 2013) and dominated by snowmelt (e.g., Ferguson 1999, Barnett et al. 2005). This effect is particularly pronounced in arctic regions (e.g., Woo 2012), which may be considered terrestrial climatic analogs to early Martian environments. The hydrograph of arctic rivers displays a peak discharge during snowmelt season (e.g., Woo 1986, Bøggild et al. 1999), and it is this peak discharge which would be responsible for the channel-forming flood. However, we lack the knowledge as to how channel dimensions controlled by snowmelt and associated peak discharges can be used to infer annual mean precipitation rates on Mars.

In summary, the condition of liquid-water precipitation is unlikely to be fulfilled. Therefore, besides the obvious discrepancy in the amount of precipitated water (e.g., Fig. 8), the fact remains that early Mars was most likely too cold to sustain network formation by continued liquid-water precipitation.

4.2. Uncertainties in surface temperature calculations

Figure 12 shows the mean precipitation as a function of CO_2 partial pressure and ΔT . It is clearly seen that even for denser atmospheres of the order of several bars, the ΔT value required for agreement in precipitation between the atmospheric model and the network data (i.e., precipitation $\geq 1.5 \text{ mm d}^{-1}$, see Fig. 8) is still of the order of 40-50 K. How could such high temperatures be achieved?

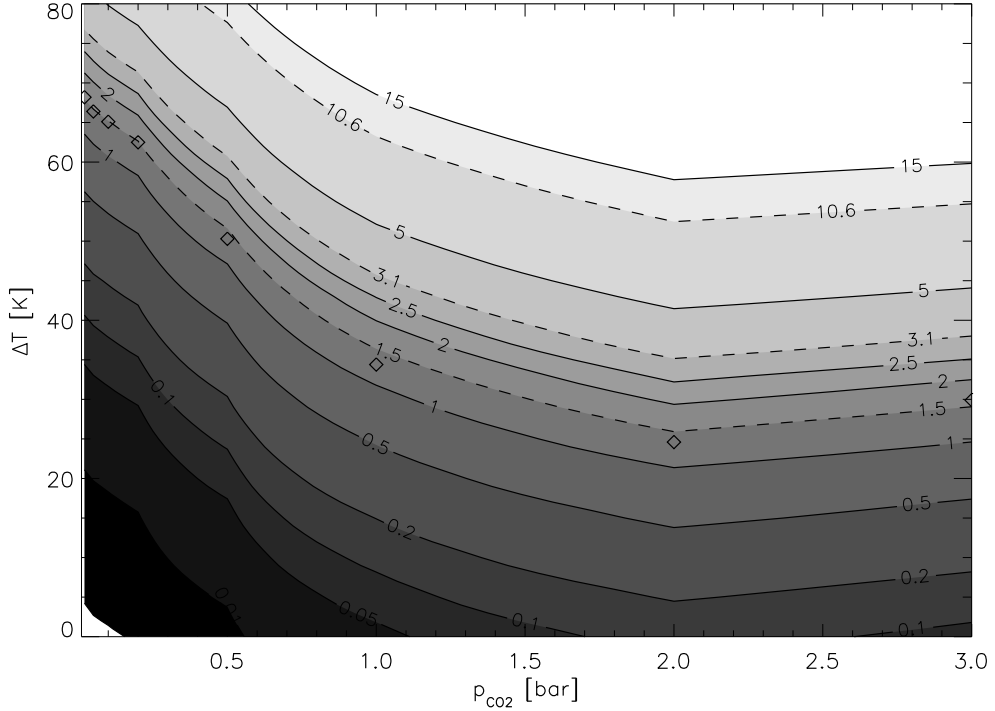


Figure 12: Mean precipitation (in mm d^{-1}) as a function of ΔT and CO_2 partial pressure (zero N_2 , $\text{RH}=1$, $p_r=13.3\%$). Dashed lines represent minimum, mean and maximum runoff as inferred from the network data. $T=273\text{ K}$ indicated by \diamond (for lower temperatures, precipitation would be in the form of snowfall). Note that the contribution of latent heat release due to evaporation is neglected, which would limit precipitation to about 1.8 mm day^{-1} (see Sect. 4.5).

4.2.1. Numerical uncertainties

Firstly, atmospheric models, hence predictions of surface temperature and precipitation, are subject to (numerical) uncertainties.

An important aspect is the radiative transfer, hence the strength of the greenhouse effect. Usually, atmospheric models do not solve the radiative transfer equation with a line-by-line code to save computational speed. They instead use faster approximations such as exponential sums or correlated-k methods (e.g., Wiscombe and Evans 1977, Goody and Yung 1989). It can be shown that such methods are quite accurate (e.g., Goody et al. 1989, West et al. 1990, Lacis and Oinas 1991), and most atmospheric models compare well to high-resolution radiative transfer calculations (e.g., Goldblatt et al. 2009, Wordsworth et al. 2010a, Ramirez et al. 2014). The impact on surface temperature is probably small, of the order of 1-2 K at most. The opacity databases which are typically employed, such as Hitran and Hitemp, have evolved quickly in recent years (e.g., Rothman et al. 2009, Rothman et al. 2013), and the effect on radiative-convective calculations can be quite important (e.g., Pavlov et al. 2000,

Kratz 2008, Kopparapu et al. 2013). Especially the treatment of line and continuum absorption of CO₂ is another uncertainty factor for early Mars calculations (e.g., Halevy et al. 2009, Wordsworth et al. 2010a, Mischna et al. 2012). Numerical issues, such as the vertical discretization of the atmospheric column, can also introduce uncertainties in surface temperature of a few K for optically thick atmospheres ($p_{CO_2} \geq 0.2-0.5$ bar). In the model used here, a warming effect of up to 7 K was observed upon increasing the number of levels in the troposphere where the opacity is largest. This effect is comparable to other 1D radiative-convective models (e.g., Tian et al. 2010, Kopparapu et al. 2013). For atmospheres with less CO₂ partial pressure, the vertical discretization is not important for the calculation of surface temperatures. In summary, we should probably assign an inherent uncertainty of 5-10 K to the calculation of mean surface temperatures. Figure 12 suggests that by using these uncertainty estimates, the discrepancy between geological data and atmospheric model estimates could increase or decrease by about 20 %.

4.2.2. 1D vs 3D models

The 1D atmospheric model used in this work calculates annual mean, global mean temperatures. However, the networks mostly formed at lower latitudes where conditions were likely warmer than such global mean values. Indeed, 3D modeling studies (e.g., Wordsworth et al. 2013, Urata and Toon 2013) have suggested that the latitudinal temperature gradient in mean surface temperature is of the order of up to 20-30 K. However, this is below the needed threshold inferred from Fig. 12.

Seasonal or obliquity effects could be much stronger (see e.g. Fig. 3 in Wordsworth et al. 2013), with temperature effects of the order of 50-60 K in some locations. Therefore, a viable alternative to a continuously wet early Mars are scenarios where obliquity cycles allow for periodic warming at the networks' geographic location which would then allow for formation and precipitation of liquid water (Wordsworth et al. 2013). This issue should be investigated with geological constraints on the valley network formation timescales. These are poorly constrained, but it seems that at least a somewhat sustained presence of water was required to form them (Ansan and Mangold 2013).

We acknowledge the importance of full 3D atmospheric studies, demonstrated for many Solar System objects, e.g. for Earth, Mars, Titan etc. However, 1D and 3D studies can be used complementarily to investigate different aspects of atmospheric processes. For example, 1D models of Titan have been used to tackle specific problems of the thermal structure (e.g., McKay et al. 1989) or haze formation (e.g., Lavvas et al. 2008a, Lavvas et al. 2008b), whereas 3D models of Titan are used to address especially the problem of (equatorial) superrotation (e.g., Hourdin et al. 1995, Friedson et al. 2009, Newman et al. 2011, Lebonnois et al. 2012). For early Mars, 1D-2D models have been used to investigate mean surface temperatures and assess the validity of greenhouse solutions (e.g., Postawko and Kuhn 1986, Pollack et al. 1987, Kasting 1991, Mischna et al. 2000, Colaprete and Toon 2003, Tian et al. 2010, Fairén et al. 2012, von Paris et al. 2013a). 3D models have demonstrated the importance of obliquity and transport effects (e.g., Johnson et al. 2008, Forget et al. 2013, Wordsworth et al. 2013, Mischna et al. 2013, Urata and Toon 2013, Scanlon et al. 2013).

It is clear that 3D models are physically more consistent than 1D models since they better resolve the planetary surface, include clouds and horizontal as well as vertical en-

ergy transport by winds or tracer species such as water. However, they introduce many parameters, some of them even on a sub-grid scale, hence parameterizations are needed (e.g., leaf area index, Fraedrich et al. 1999, or surface roughness, Wordsworth et al. 2013). Other parameters include, e.g., precipitation efficiencies or precipitation thresholds, cloud properties and the amount of cloud nuclei (e.g., Wordsworth et al. 2013). Most of them are not known for early Mars.

On applying 3D models, one should always bear in mind that the boundary conditions might so uncertain that one could be simulating conditions which are very different.

In contrast, 1D models somewhat keep the number of parameters under control. In our model as used for the current manuscript, effectively, the only parameters are the choice of surface albedo and the choice of the RH profile.

In addition, the current spatial latitude-longitude resolution of most 3D GCM studies of early Mars (e.g., 32x24 or 32x32 in Wordsworth et al. 2013 and Forget et al. 2013) is insufficient to resolve individual networks. Therefore, even 3D GCM simulations would probably not be enough to address the question of local precipitation for individual networks.

As stated in the Introduction, we aim at assessing the general strength of the early Mars hydrological cycle, and not individual network channels. Therefore, the choice of a 1D model is not thought to severely impact our conclusions.

Ideally, for Early Mars, one would apply both 3D snapshots of the obliquity cycle to investigate the detailed feedback mechanisms, as well as 1D studies to investigate a wide parameter range (of e.g. atmospheric composition) not possible in 3D. In our present work, a 1D study is used to provide only basic indications of the hydrologic cycle, which in turn depend on obliquity etc. Such a two-pronged approach (i.e. complementary 1D and 3D studies) could in our opinion prove beneficial for Early Mars.

4.2.3. Atmospheric composition

In the global mean, von Paris et al. (2013a) suggested that 500 mbar of N₂ would provide about 10 K surface warming. Other candidates for providing surface warming are additional greenhouse gases such as CH₄ and SO₂ (e.g., Postawko and Kuhn 1986, Yung et al. 1997, Johnson et al. 2008, Tian et al. 2010, Mischna et al. 2013). However, an unresolved question is the possible formation of aerosols due to high SO₂ concentrations. Like O₃ (a possible by-product of CO₂ photochemistry, e.g. Selsis et al. 2002), SO₂ is a strong UV absorber. This could help to avoid the surface cooling due to CO₂ Rayleigh scattering observed at high surface pressures, since SO₂ or O₃ absorption bands would strongly reduce the planetary albedo (e.g., von Paris et al. 2013b). Furthermore, together with near-IR CH₄ absorption, such trace gases would probably warm the lower stratosphere such that CO₂ cloud formation would be largely inhibited, thus reducing the cloud radiative forcing. Volcanic gases such as H₂ could also play a role in warming early Mars since collision-induced absorption could provide a large greenhouse effect, and Rayleigh scattering of H₂ is far less efficient than for CO₂ (e.g., Stevenson 1999, Pierrehumbert and Gaidos 2011, Wordsworth et al. 2011, Wordsworth and Pierrehumbert 2013, Ramirez et al. 2014). The study of Ramirez et al. (2014) found mean surface temperatures at high CO₂ partial pressures which are compatible with the network data presented here.

4.3. Uncertainties in the estimation of discharge and runoff

Our estimates of discharge and the inferred precipitation rates are subject to large uncertainties. The simple assumption that discharge rates can be used to directly estimate precipitation rates neglects many important factors that control this relationship. In this section we address some of the uncertainties that are necessarily involved in attempts to reconstruct the water budget in a 3.8 Gyr-old catchment.

4.3.1. Discharge calculations

Previous studies used different approaches to estimate paleodischarges of Martian channels. Ideally, reliable estimates of paleodischarge would require not only the measurement of morphometric properties of channels, but also the knowledge of or at least well-constrained assumptions of other, independent parameters such as particle size distributions of mobilized sediment and channel floor roughness (see review by Kleinhans 2005). The input parameters for such micro-scale or hydraulic methods are usually poorly known for modern Mars, since they cannot be easily obtained from orbit. However, they can be measured in situ by rovers such as MSL/Curiosity, which landed on the distal parts of an alluvial fan in Gale Crater. For example, the size distribution of rounded and fluvially transported particles was determined by Yingst et al. (2013). The flow velocity, water depth, and discharge of channels that transported the particles that now form outcrops of conglomerate was estimated by Williams et al. (2013). Nevertheless, the data limitations for most other Martian channels imply that macro-scale or hydrologic methods need to be applied for paleodischarge estimates (see Burr et al. 2010). Such form-discharge approaches are based on morphological parameters that are relatively simple to measure and have been used extensively (e.g., Irwin et al. 2005, Williams et al. 2013). It is important to note, however, that gravity effects (e.g., on channel geometry) and the unknown strength of channel banks on Mars introduce significant errors to our paleodischarge estimates (Williams et al. 2013). Moreover, as mentioned, since we usually cannot measure the channel width, we use an empirical relation of channel width to valley width (see Eq. 10).

From eq. 9, the uncertainty $\frac{\Delta R}{R}$ of the calculated runoff is given by

$$\left(\frac{\Delta R}{R}\right)^2 = \left(\frac{\Delta C}{C}\right)^2 + \left(\frac{\Delta Q}{Q}\right)^2 \quad (12)$$

The uncertainty $\frac{\Delta Q}{Q}$ is partly due to the measurement error $\frac{\Delta W_v}{W_v}$ associated with the channel or valley width. However, a very significant part is also contributed by uncertainties due to the application of the approximative eqs. 6 (U_6 , for deriving discharges) and 10 (U_{10} , for deriving channel widths). Combining these, we find

$$\left(\frac{\Delta R}{R}\right)^2 = \left(\frac{\Delta C}{C}\right)^2 + \left(1.71 \cdot \frac{\Delta W_C}{W_C}\right)^2 + U_6^2 + U_{10}^2 \quad (13)$$

For a conservative estimate of a 20% error in the measurements of both catchment area and channel width, and taking $U_6=0.79$ (standard error for applying the power law of eq. 6 to discharge calculations, Table 3 in Osterkamp and Hedman 1982) and $U_{10}=0.1$ (interquartile range for the proportionality constant in eq. 10, Penido et al.

2013), we thus assign a 1σ error of 90% to the calculated runoff. Note that this neglects any potential systematic uncertainty from applying eq. 10, implying that our runoff uncertainty estimates are probably optimistic.

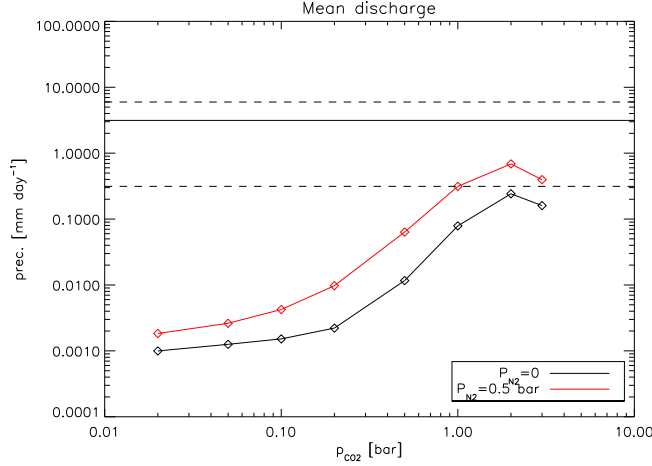


Figure 13: Median network runoff (plain line) with its 1σ error of 90%, (dashed lines) compared to total model precipitation (mm d^{-1}) with nominal values of $\text{RH}=1$ and $pr=13.3\%$. Black: No N_2 , red: 0.5 bar N_2 .

Figure 13 shows the effect of this error estimate on the comparison between atmospheric model precipitation and derived network runoff. For high-pressure atmospheres with significant amounts of N_2 , both data sets seem to compare roughly within error bars. Note, however, that our 1D steady-state model atmospheres predict snowfall rather than rainfall (see surface temperatures in Fig. 1), hence, the associated runoff would be zero.

Another error source stems from the fact that the approximation formulae provided by Osterkamp and Hedman (1982) were derived for the Missouri river basin. For other basins, such formulae will probably differ, although, as stated by Osterkamp and Hedman (1982), a large number of individual river channels were included in the analysis. Therefore, data are expected to cover a wide range of channel widths and discharge values, and the total scatter is probably not much larger than the already stated 79%.

4.3.2. Role of evaporation and infiltration

The derivation of precipitation rates from channel discharge rates (assuming the channel banks are full) is far from being straightforward. First, the area of the catchment must be known, the shape of which may have been changed by erosion or tectonic deformation in the last ~ 3.8 Gyr. Additional uncertainties may arise from data limitations during the mapping process (Penido et al. 2013). Second, drainage in a channel does not directly correspond to runoff or precipitation in its catchment area. If discharge is used to infer precipitation rates, the relative roles of evaporation and infiltration need to be considered (transpiration does not exist on Mars since there is no vegetation). In general, the water balance in a catchment system can be expressed as

$$\Delta S = P - Q_S - Q_G - ET \quad (14)$$

where ΔS is the change in the amount of water stored in the system, P is rainfall, i.e. liquid water precipitation, Q_S is surface discharge, Q_G is groundwater discharge, and ET is evapotranspiration. For practical purposes, the amount of water in a system is often assumed to be constant. In terrestrial hydrological studies, infiltration is often considered to be negligible (Anderson and Anderson 2010), since the infiltrated water returns to the stream system as groundwater. If the overall climate is cold (Wordsworth et al. 2013) and the substrate in which a channel is incised is subject to permafrost, the infiltration rate would even tend towards zero, because a permafrost ground would, to a first order, be impermeable (see also Heldmann et al. 2005). Applying the same logic to Mars, we can thus consider Eq. 14 to be equivalent to

$$\int (R - E) dt = \frac{1}{A} \int Q_S dt \quad (15)$$

with R is the rainfall rate, Q_S the hydrograph and A the area of catchment. Evaporation and sublimation rates on modern Mars have been estimated by several past studies. Chittenden et al. (2008) determined sublimation rates of pure water ice as a function of temperature, wind speed, and relative humidity. They found that temperature is the main factor influencing the sublimation rate. The results of Chittenden et al. (2008) show sublimation rates of less than a millimeter per hour (see Table 2 of Chittenden et al. 2008). Whereas these results apply to water ice, Sears and Moore (2005) performed laboratory experiments with a 7 mbar CO_2 atmosphere at 0°C and obtained evaporation rates of $1.01 \pm 0.19 \text{ mm h}^{-1}$. After a correction for gravity effects, Sears and Moore (2005) predict evaporation rates on Mars of $0.73 \pm 0.14 \text{ mm h}^{-1}$. If one assumes that runoff took place in a rather cold environment on early Mars (Wordsworth et al. 2013), then both sublimation of ice and evaporation of liquid water may have occurred. The effect of thin water ice layers with temperatures around the freezing point of water were investigated by Moore and Sears (2006). These authors find evaporation rates of $0.84 \pm 0.08 \text{ mm h}^{-1}$ and $1.24 \pm 0.12 \text{ mm h}^{-1}$ with and without a thin ice layer, respectively, and conclude that the presence of thin water ice layers does not have a significant effect on the evaporation rates. The corresponding values for a whole day are 2.02 and 2.98 cm d^{-1} with and without a thin ice layer, respectively. These rates are of the same order of magnitude as those obtained from discharge estimates, and therefore have to be taken into account and need to be added to the discharge-derived rate before calculating precipitation rates. Of course, the catchment would not be a free surface of water, in which case evaporation rates may be somewhat lower than those obtained for free water surfaces, but in any case the amount of evaporated water would not be negligible.

Another question is whether the assumption of insignificant infiltration in Eq. 14 is valid. The upper crust in the southern highlands, where the valley networks are observed, probably consists of heavily cratered regolith. Such substrate would be characterized by high infiltration capacities that may have impeded runoff production (e.g., Baker and Partridge 1986, Gulick and Baker 1990, Grant and Schultz 1993, Carr and Malin 2000, Irwin et al. 2008 and references therein). In a study of a terres-

trial analogue on Hawaii at the Kilauea and Kaù deserts, which are characterized by brecciated basaltic material, Craddock et al. (2012) estimate that runoff can only be generated if precipitation rates are $>2.5 \text{ cm h}^{-1}$. Infiltrated water would feed groundwater aquifers, which in turn may have contributed to the generation of sapping valleys by groundwater seepage. Groundwater flow, however, may have been different to surface runoff and its associated catchment areas, and it is unclear how to quantify this effect. Since the mean annual temperatures indicated by our study (Fig. 1) and previous modeling of early Mars temperatures (Wordsworth et al. 2013) are below 0°C , we assume permafrost conditions in our hydrologic estimates and therefore neglect the effects of infiltration, including the possible (but minor) infiltration of snow melt into frozen ground.

The above comparison between geomorphologic data and atmospheric models (see e.g., Fig.8) explicitly assumes no infiltration and no evaporation, i.e. all precipitated water would feed the valley network runoff. Even under such optimistic assumptions, there is a disagreement between both methods. Hence, it is clear that a more detailed analysis, taking into account the full eq. 14, would most likely lead to a larger disagreement. However, given the uncertainties in runoff estimates (see Fig. 13), a full hydrological analysis is probably not warranted by the current data quality.

4.4. Dry warm Mars?

Mean surface temperatures above freezing (warm Mars) do not necessarily lead to high precipitation (wet Mars). Paleoclimate studies of the Earth during phases of large super-continent imply that the continental climate during these phases might have been very dry (Parrish 1993). This suggests that another condition for extensive precipitation on early Mars would be the presence of large standing bodies of liquid water. 3D climate studies of, e.g., Soto (2012) suggest that without a large ocean, early Mars would have been extremely arid even if it was warm. The existence of a Noachian ocean is currently debated. Several studies however advocate that the northern lowlands have been at least partly ocean-covered (e.g., Clifford and Parker 2001, Perron et al. 2007, Dibiase et al. 2013, De Blasio 2014). If indeed such a large ocean would have existed, precipitation on a warm early Mars would have been abundant (Soto 2012).

4.5. Limits to evaporation

Liquid-water precipitation must be balanced by evaporation of surface water into the atmosphere, otherwise the water column will deplete quickly. Evaporation then leads to a cooling of the surface through the release of latent heat (e.g., Fraedrich et al. 1999). In the model used here, this latent heat flux F_{lat} is neglected, and the surface energy balance is only determined by the radiative flux F_{rad} . However, for increasing amounts of evaporation, the contribution of F_{lat} can become significant, and the surface energy balance should read as

$$F_{\text{surf}} = F_{\text{rad}} + F_{\text{lat}} \quad (16)$$

The radiative flux in eq. 16 is determined by the net stellar flux reaching the surface and the radiative longwave cooling (i.e., downwards-upwards longwave fluxes). It is calculated directly in the atmospheric model.

For high-pressure atmospheres, the greenhouse effect becomes strong, and the longwave cooling is close to 0 (see von Paris et al. 2013a). For surface pressures higher than about 0.5 bar, the surface radiative flux is almost entirely dominated by the stellar flux.

The right panel of Fig. 14 shows the latent heat flux of the precipitation rates as taken from Fig. 8, assuming a latent heat of $2,500 \text{ J g}^{-1}$. It is clearly seen that except the high- CO_2 runs ($p > 1 \text{ bar}$), the value of F_{lat} is somewhat negligible, justifying the model assumption of taking only the radiative flux into account.

In an approach similar to O’Gorman and Schneider (2008), the left panel of Fig. 14 shows the maximum of global mean precipitation, if the entire net surface radiative flux of the model atmospheres would be used to evaporate water. Also indicated are the values of precipitation from Table 1. Furthermore, the dotted horizontal line shows the absolute global mean maximum of precipitation ($\approx 3.8 \text{ mm day}^{-1}$), if the entire top-of-atmosphere incoming stellar flux ($\approx 109 \text{ W m}^{-2}$) would be available for surface water evaporation. This is equivalent to assuming a zero-albedo atmosphere (no absorption or scattering of radiation), which is clearly not realistic, as indicated in Fig. 1. Furthermore, longwave cooling as well as surface reflectivity would have to be zero as well, which would be mutually inconsistent. In addition, such a scenario would need a global ocean which is questionable (see discussion above in Sect. 4.4).

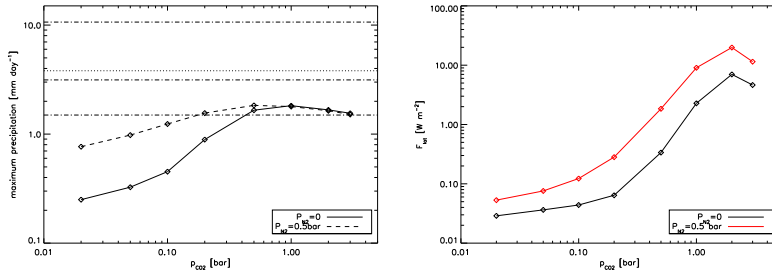


Figure 14: Left: Maximum global mean precipitation based on surface energy balance. Network maximum, minimum and median indicated by dot-dashed horizontal lines. Dotted horizontal line indicates maximum precipitation for zero-albedo atmosphere. Right: Latent heat flux of precipitation rates from Fig. 8.

In summary, these calculations suggest that the maximum global mean precipitation sustainable under the faint-Sun conditions assumed for early Mars is about 1.8 mm day^{-1} (Fig. 14, left panel). This is still much less than inferred precipitation from the valley network analysis. Accounting for a latitudinal or seasonal gradient in precipitation compared to a global mean (see discussions above and eq. 4), this could have been enough to sustain valley network formation, even if barely for the highest-runoff channels. However, given that such an amount of precipitation requires that all of the stellar energy reaching the surface be converted into latent heat, these highest-runoff channels were probably not formed during long, continuously wet periods.

5. Conclusions

In this work, we have estimated runoff rates for 18 Mars valley networks and compared them to estimated precipitation rates from an atmospheric model of early Mars. Model atmospheres were composed of varying amounts of CO₂ and N₂. We also varied parameters such as atmospheric relative humidity and precipitation efficiency to estimate their impact on precipitation values.

Runoff rates inferred from valley network data and precipitation from the atmospheric model generally disagree by about an order of magnitude for high-pressure CO₂ atmospheres, the runoff rates being much larger than the atmospheric model precipitation rates. At low CO₂ partial pressures, a scenario favored by escape models, the discrepancy is even larger. This suggests that early Mars was probably not a continuously wet environment. Rather, these results point to sporadic periods of high precipitation, probably due to a change in obliquity, or, more likely, (local) melting events where a large snow/ice reservoir accumulated over a geologically long time (e.g., an obliquity cycle) could have melted in a short period. Even though such a conclusion is not new, it is the first time that both geological and atmospheric modeling approaches have been used to test quantitatively the hypothesis of wet versus dry early Mars.

Geological runoff rates are uncertain by currently at least 90% and atmospheric models are also subject to uncertainties. Therefore, quantitatively comparing the estimates of the amount of precipitated water from both approaches is challenging. However, since global mean surface temperatures as calculated by our atmospheric modeling are far below freezing, calculated model precipitation is most likely not a good predictor of valley network runoff. This points the direction of future research, i.e. the need to better constrain estimates of paleo-discharges in ancient river networks on early Mars, determine the water source for runoff (e.g., snowmelt or rain) and its timescales and refine mesoscale atmospheric modeling of early Mars climate before more rigorous conclusions can be drawn.

Nevertheless our study represents an important first step in constraining precipitation on early Mars involving both the atmospheric and geological communities.

Acknowledgements

This study has received financial support from the French State in the frame of the "Investments for the future" Programme IdEx Bordeaux, reference ANR-10-IDEX-03-02. This research has been supported by the Helmholtz Association through the research alliance "Planetary Evolution and Life". We thank two anonymous reviewers for stimulating comments. Discussions with Mareike Godolt, Franck Selsis and Franck Hersant are gratefully acknowledged. Discussions with Robert Craddock have sharpened our view on infiltration rates on Mars.

References

- R. F. Adler, G. Gu, and G. J. Huffman. Estimating Climatological Bias Errors for the Global Precipitation Climatology Project (GPCP). *J. Applied Meteorology and Climatology*, 51:84–99, January 2012. doi: 10.1175/JAMC-D-11-052.1.

- R. Anderson and S. Anderson. *Geomorphology*. Cambridge University Press, Cambridge, 2010.
- V. Ansan and N. Mangold. 3D morphometry of valley networks on Mars from HRSC/MEX DEMs: Implications for climatic evolution through time. *J. Geophys. Res.(Planets)*, 118:1873–1894, October 2013. doi: 10.1002/jgre.20117.
- V. R. Baker and J. B. Partridge. Small Martian valleys - Pristine and degraded morphology. *J. Geophys. Res.*, 91:3561–3572, March 1986. doi: 10.1029/JB091iB03p03561.
- T. P. Barnett, J. C. Adam, and D. P. Lettenmaier. Potential impacts of a warming climate on water availability in snow-dominated regions. *Nature*, 438:303–309, November 2005. doi: 10.1038/nature04141.
- C. J. Barnhart, A. D. Howard, and J. M. Moore. Long-term precipitation and late-stage valley network formation: Landform simulations of Parana Basin, Mars. *J. Geophys. Res.(Planets)*, 114:E01003, January 2009. doi: 10.1029/2008JE003122.
- M. Bavay, M. Lehning, T. Jonas, and H. Löwe. Simulations of future snow cover and discharge in Alpine headwater catchments. *Hydrological Processes*, 23:95–108, January 2009. doi: 10.1002/hyp.7195.
- C. E. Bøggild, C. J. Knudby, M. B. Knudsen, and W. Starzer. Snowmelt and runoff modelling of an Arctic hydrological basin in west Greenland. *Hydrological Processes*, 13:1989–2002, September 1999. doi: 10.1002/(SICI)1099-1085(199909)13:12/13<1989::AID-HYP848>3.0.CO;2-Y.
- P. Buhler, C. Fassett, J. Head, and M. Lamb. Timescales of Fluvial Activity and Intermittency in Milna Crater, Mars. *accepted in Icarus*, 2014. doi: 10.1016/j.icarus.2014.06.028.
- D. M. Burr, R. M. E. Williams, K. D. Wendell, M. Chojnacki, and J. P. Emery. Inverted fluvial features in the Aeolis/Zephyria Plana region, Mars: Formation mechanism and initial paleodischarge estimates. *J. Geophys. Res.(Planets)*, 115:E07011, July 2010. doi: 10.1029/2009JE003496.
- M. H. Carr. The Martain drainage system and the origin of valley networks and fretted channels. *J. Geophys. Res.*, 100:7479–7507, April 1995. doi: 10.1029/95JE00260.
- M. H. Carr and J. W. Head. Geologic history of Mars. *Earth Plan. Science Letters*, 294:185–203, June 2010. doi: 10.1016/j.epsl.2009.06.042.
- M. H. Carr and M. C. Malin. Meter-Scale Characteristics of Martian Channels and Valleys. *Icarus*, 146:366–386, August 2000. doi: 10.1006/icar.2000.6428.
- J. D. Chittenden, V. Chevrier, L. A. Roe, K. Bryson, R. Pilgrim, and D. W. G. Sears. Experimental study of the effect of wind on the stability of water ice on Mars. *Icarus*, 196:477–487, August 2008. doi: 10.1016/j.icarus.2008.01.016.

- S. M. Clifford and T. J. Parker. The Evolution of the Martian Hydrosphere: Implications for the Fate of a Primordial Ocean and the Current State of the Northern Plains. *Icarus*, 154:40–79, November 2001. doi: 10.1006/icar.2001.6671.
- G. D. Clow. Generation of liquid water on Mars through the melting of a dusty snowpack. *Icarus*, 72:95–127, October 1987. doi: 10.1016/0019-1035(87)90123-0.
- A. Colaprete and O. B. Toon. Carbon dioxide clouds in an early dense Martian atmosphere. *J. Geophys. Res.*, 108:6–1, April 2003. doi: 10.1029/2002JE001967.
- R. A. Craddock and A. D. Howard. The case for rainfall on a warm, wet early Mars. *J. Geophys. Res.(Planets)*, 107:5111, November 2002. doi: 10.1029/2001JE001505.
- R. A. Craddock, A. D. Howard, R. P. Irwin, III, S. Tooth, R. M. E. Williams, and P.-S. Chu. Drainage network development in the Keanakoi tephra, Kilauea Volcano, Hawaii: Implications for fluvial erosion and valley network formation on early Mars. *J. Geophys. Res.(Planets)*, 117:E08009, August 2012. doi: 10.1029/2012JE004074.
- F. V. De Blasio. Possible erosion marks of bottom oceanic currents in the northern lowlands of Mars. *Planet. Space Science*, 93:10–21, April 2014. doi: 10.1016/j.pss.2014.01.014.
- D. de Niem, E. Kührt, A. Morbidelli, and U. Motschmann. Atmospheric erosion and replenishment induced by impacts upon the Earth and Mars during a heavy bombardment. *Icarus*, 221:495–507, November 2012. doi: 10.1016/j.icarus.2012.07.032.
- R. A. Dibiasi, A. B. Limaye, J. S. Scheingross, W. W. Fischer, and M. P. Lamb. Deltaic deposits at Aeolis Dorsa: Sedimentary evidence for a standing body of water on the northern plains of Mars. *J. Geophys. Res.Planets*, 118:1285–1302, June 2013. doi: 10.1002/jgre.20100.
- A. G. Fairén, J. D. Haqq-Misra, and C. P. McKay. Reduced albedo on early Mars does not solve the climate paradox under a faint young Sun. *Astron. Astrophys.*, 540:A13, April 2012. doi: 10.1051/0004-6361/201118527.
- J. Farquhar, J. Savarino, T. L. Jackson, and M. H. Thiemens. Evidence of atmospheric sulphur in the martian regolith from sulphur isotopes in meteorites. *Nature*, 404: 50–52, March 2000.
- C. I. Fassett and J. W. Head. The timing of martian valley network activity: Constraints from buffered crater counting. *Icarus*, 195:61–89, May 2008. doi: 10.1016/j.icarus.2007.12.009.
- C. I. Fassett and J. W. Head. Sequence and timing of conditions on early Mars. *Icarus*, 211:1204–1214, February 2011. doi: 10.1016/j.icarus.2010.11.014.
- C. I. Fassett and J. W. Head, III. Valleys on Hecates Tholus, Mars: origin by basal melting of summit snowpack. *Planet. Space Science*, 54:370–378, April 2006. doi: 10.1016/j.pss.2005.12.011.

- C. I. Fassett, J. L. Dickson, J. W. Head, J. S. Levy, and D. R. Marchant. Supraglacial and proglacial valleys on Amazonian Mars. *Icarus*, 208:86–100, July 2010. doi: 10.1016/j.icarus.2010.02.021.
- R. Ferguson. Snowmelt runoff models. *Prog. Phys. Geogr.*, 23:205–227, 1999. doi: 10.1177/030913339902300203.
- F. Forget and R. T. Pierrehumbert. Warming Early Mars with Carbon Dioxide Clouds That Scatter Infrared Radiation. *Science*, 278:1273–1276, November 1997.
- F. Forget, R. Wordsworth, E. Millour, J.-B. Madeleine, L. Kerber, J. Leconte, E. Marcq, and R. M. Haberle. 3D modelling of the early martian climate under a denser CO₂ atmosphere: Temperatures and CO₂ ice clouds. *Icarus*, 222:81–99, January 2013. doi: 10.1016/j.icarus.2012.10.019.
- J. L. Fox and A. Hać. Isotope fractionation in the photochemical escape of O from Mars. *Icarus*, 208:176–191, July 2010. doi: 10.1016/j.icarus.2010.01.019.
- K. Fraedrich, A. Kleidon, and F. Lunkeit. A Green Planet versus a Desert World: Estimating the Effect of Vegetation Extremes on the Atmosphere. *Journal of Climate*, 12:3156–3163, October 1999. doi: 10.1175/1520-0442(1999)012<3156:AGPVAD>2.0.CO;2.
- A. J. Friedson, R. A. West, E. H. Wilson, F. Oyafuso, and G. S. Orton. A global climate model of Titan’s atmosphere and surface. *Planet. Space Science*, 57:1931–1949, December 2009. doi: 10.1016/j.pss.2009.05.006.
- C. Gillmann, P. Lognonné, and M. Moreira. Volatiles in the atmosphere of Mars: The effects of volcanism and escape constrained by isotopic data. *Earth Plan. Science Letters*, 303:299–309, March 2011. doi: 10.1016/j.epsl.2011.01.009.
- C. Goldblatt, T. Lenton, and A. Watson. An evaluation of the long-wave radiative transfer code used in the Met Office Unified Model. *Qart. J. Royal Met. Soc.*, 135: 619–633, 2009. doi: 10.1002/qj.403.
- J. M. Goldspiel and S. W. Squyres. Groundwater Sapping and Valley Formation on Mars. *Icarus*, 148:176–192, November 2000. doi: 10.1006/icar.2000.6465.
- R. Goody, R. West, L. Chen, and D. Crisp. The correlated-k method for radiation calculations in nonhomogeneous atmospheres. *J. Quant. Spect. Rad. Trans.*, 42: 539–550, December 1989.
- R. M. Goody and Y. L. Yung. *Atmospheric radiation : Theoretical basis*. Atmospheric radiation : theoretical basis, 2nd ed., by Richard M. Goody and Y.L. Yung. New York, NY: Oxford University Press, 1989.
- D. O. Gough. Solar interior structure and luminosity variations. *Solar Physics*, 74: 21–34, November 1981. doi: 10.1007/BF00151270.
- J. A. Grant and P. H. Schultz. Degradation of selected terrestrial and Martian impact craters. *J. Geophys. Res.*, 98:11025, June 1993. doi: 10.1029/93JE00121.

- J. L. Grenfell, B. Stracke, P. von Paris, B. Patzer, R. Titz, A. Segura, and H. Rauer. The response of atmospheric chemistry on earthlike planets around F, G and K Stars to small variations in orbital distance. *Planet. Space Science*, 55:661–671, April 2007. doi: 10.1016/j.pss.2006.09.002.
- M. Grott, A. Morschhauser, D. Breuer, and E. Hauber. Volcanic outgassing of CO₂ and H₂O on Mars. *Earth Plan. Science Letters*, 308:391–400, August 2011. doi: 10.1016/j.epsl.2011.06.014.
- V. C. Gulick and V. R. Baker. Origin and evolution of valleys on Martian volcanoes. *J. Geophys. Res.*, 95:14325–14344, August 1990. doi: 10.1029/JB095iB09p14325.
- K. Gwinner, F. Scholten, F. Preusker, S. Elgner, T. Roatsch, M. Spiegel, R. Schmidt, J. Oberst, R. Jaumann, and C. Heipke. Topography of Mars from global mapping by HRSC high-resolution digital terrain models and orthoimages: Characteristics and performance. *Earth Plan. Science Letters*, 294:506–519, June 2010. doi: 10.1016/j.epsl.2009.11.007.
- I. Halevy, M. T. Zuber, and D. P. Schrag. A Sulfur Dioxide Climate Feedback on Early Mars. *Science*, 318:1903–, December 2007. doi: 10.1126/science.1147039.
- I. Halevy, R. T. Pierrehumbert, and D. P. Schrag. Radiative transfer in CO₂-rich paleoatmospheres. *J. Geophys. Res.*, 114:18112, September 2009. doi: 10.1029/2009JD011915.
- K. P. Harrison and R. E. Grimm. Groundwater-controlled valley networks and the decline of surface runoff on early Mars. *J. Geophys. Res.(Planets)*, 110:E12S16, October 2005. doi: 10.1029/2005JE002455.
- E. Hauber, T. Platz, D. Reiss, L. Le Deit, M. G. Kleinhans, W. A. Marra, T. Haas, and P. Carbonneau. Asynchronous formation of Hesperian and Amazonian-aged deltas on Mars and implications for climate. *J. Geophys. Res.*, 118:1529–1544, July 2013. doi: 10.1002/jgre.20107.
- J. L. Heldmann, O. B. Toon, W. H. Pollard, M. T. Mellon, J. Pitlick, C. P. McKay, and D. T. Andersen. Formation of Martian gullies by the action of liquid water flowing under current Martian environmental conditions. *J. Geophys. Res.(Planets)*, 110: E05004, May 2005. doi: 10.1029/2004JE002261.
- D. E. J. Hobley, A. D. Howard, and J. M. Moore. Fresh shallow valleys in the Martian midlatitudes as features formed by meltwater flow beneath ice. *J. Geophys. Res.*, 119:128–153, January 2014. doi: 10.1002/2013JE004396.
- M. R. T. Hoke and B. M. Hynek. Roaming zones of precipitation on ancient Mars as recorded in valley networks. *J. Geophys. Res.(Planets)*, 114:E08002, August 2009. doi: 10.1029/2008JE003247.
- M. R. T. Hoke, B. M. Hynek, and G. E. Tucker. Formation timescales of large Martian valley networks. *Earth Plan. Science Letters*, 312:1–12, December 2011. doi: 10.1016/j.epsl.2011.09.053.

- F. Hourdin, O. Talagrand, R. Sadourny, R. Courtin, D. Gautier, and C. P. McKay. Numerical simulation of the general circulation of the atmosphere of Titan. *Icarus*, 117: 358–374, October 1995. doi: 10.1006/icar.1995.1162.
- A. D. Howard and J. M. Moore. Late Hesperian to early Amazonian midlatitude Martian valleys: Evidence from Newton and Gorgonum basins. *J. Geophys. Res.*, 116: E05003, May 2011. doi: 10.1029/2010JE003782.
- B. M. Hynek, M. Beach, and M. R. T. Hoke. Updated global map of Martian valley networks and implications for climate and hydrologic processes. *J. Geophys. Res.(Planets)*, 115:E09008, September 2010. doi: 10.1029/2009JE003548.
- R. P. Irwin, A. D. Howard, R. A. Craddock, and J. M. Moore. An intense terminal epoch of widespread fluvial activity on early Mars: 2. Increased runoff and paleolake development. *J. Geophys. Res.(Planets)*, 110:E12S15, December 2005. doi: 10.1029/2005JE002460.
- R. P. Irwin, A. D. Howard, and R. A. Craddock. Fluvial valley networks on Mars. In *River confluences, Tributaries, and the Fluvial Network*, pages 419–451. Wiley, December 2008.
- B. M. Jakosky and R. J. Phillips. Mars’ volatile and climate history. *Nature*, 412: 237–244, July 2001.
- R. Jaumann, D. Reiss, S. Frei, G. Neukum, F. Scholten, K. Gwinner, T. Roatsch, K.-D. Matz, V. Mertens, E. Hauber, H. Hoffmann, U. Köhler, J. W. Head, H. Hiesinger, and M. H. Carr. Interior channels in Martian valleys: Constraints on fluvial erosion by measurements of the Mars Express High Resolution Stereo Camera. *Geophys. Res. Letters*, 32:L16203, August 2005. doi: 10.1029/2005GL023415.
- R. Jaumann, G. Neukum, T. Behnke, T. C. Duxbury, K. Eichentopf, J. Flohrer, S. v. Gasselt, B. Giese, K. Gwinner, E. Hauber, H. Hoffmann, A. Hoffmeister, U. Köhler, K.-D. Matz, T. B. McCord, V. Mertens, J. Oberst, R. Pischel, D. Reiss, E. Ress, T. Roatsch, P. Saiger, F. Scholten, G. Schwarz, K. Stephan, M. Wählisch, and the HRSC Co-Investigator Team. The high-resolution stereo camera (HRSC) experiment on Mars Express: Instrument aspects and experiment conduct from interplanetary cruise through the nominal mission. *Planet. Space Science*, 55:928–952, May 2007. doi: 10.1016/j.pss.2006.12.003.
- R. Jaumann, A. Nass, D. Tirsch, D. Reiss, and G. Neukum. The Western Libya Montes Valley System on Mars: Evidence for episodic and multi-genetic erosion events during the Martian history. *Earth Plan. Science Letters*, 294:272–290, June 2010. doi: 10.1016/j.epsl.2009.09.026.
- S. S. Johnson, M. A. Mischna, T. L. Grove, and M. T. Zuber. Sulfur-induced greenhouse warming on early Mars. *J. Geophys. Res.*, 113:8005, August 2008. doi: 10.1029/2007JE002962.

- M. A. Kahre, S. K. Vines, R. M. Haberle, and J. L. Hollingsworth. The early Martian atmosphere: Investigating the role of the dust cycle in the possible maintenance of two stable climate states. *J. Geophys. Res.(Planets)*, 118:1388–1396, June 2013. doi: 10.1002/jgre.20099.
- E. Kalnay, M. Kanamitsu, R. Kistler, W. Collins, D. Deaven, L. Gandin, M. Iredell, S. Saha, G. White, J. Woollen, Y. Zhu, A. Leetmaa, B. Reynolds, M. Chelliah, W. Ebisuzaki, W. Higgins, J. Janowiak, K. C. Mo, C. Ropelewski, J. Wang, R. Jenne, and D. Joseph. The NCEP/NCAR 40-Year Reanalysis Project. *Bull. Amer. Meteor. Soc.*, 77:437–472, March 1996. doi: 10.1175/1520-0477(1996)077<0437:TNYRP>2.0.CO;2.
- J. F. Kasting. CO₂ condensation and the climate of early Mars. *Icarus*, 94:1–13, November 1991. doi: 10.1016/0019-1035(91)90137-1.
- J. F. Kasting, D. P. Whitmire, and R. T. Reynolds. Habitable Zones around Main Sequence Stars. *Icarus*, 101:108–128, January 1993. doi: 10.1006/icar.1993.1010.
- E. S. Kite, I. Halevy, M. A. Kahre, M. J. Wolff, and M. Manga. Seasonal melting and the formation of sedimentary rocks on Mars, with predictions for the Gale Crater mound. *Icarus*, 223:181–210, March 2013. doi: 10.1016/j.icarus.2012.11.034.
- E. S. Kite, J.-P. Williams, A. Lucas, and O. Aharonson. Low palaeopressure of the martian atmosphere estimated from the size distribution of ancient craters. *Nature Geoscience*, 7:335–339, May 2014. doi: 10.1038/ngeo2137.
- D. Kitzmann, A. B. C. Patzer, and H. Rauer. Clouds in the atmospheres of extrasolar planets. IV. On the scattering greenhouse effect of CO₂ ice particles: Numerical radiative transfer studies. *Astron. Astrophys.*, 557:A6, September 2013. doi: 10.1051/0004-6361/201220025.
- M. G. Kleinhans. Flow discharge and sediment transport models for estimating a minimum timescale of hydrological activity and channel and delta formation on Mars. *J. Geophys. Res.(Planets)*, 110:E12003, December 2005. doi: 10.1029/2005JE002521.
- R. Kopparapu, R. Ramirez, J. Kasting, V. Eymet, T. D. Robinson, S. Mahadevan, R. C. Terrien, S. Domagal-Goldman, V. Meadows, and R. Deshpande. Habitable Zones Around Main-Sequence Stars: New Estimates. *Astrophys. J.*, 765(2):131, February 2013. doi: doi:10.1088/0004-637X/765/2/131.
- D. P. Kratz. The sensitivity of radiative transfer calculations to the changes in the HITRAN database from 1982 to 2004. *J. Quant. Spect. Rad. Trans.*, 109:1060–1080, April 2008. doi: 10.1016/j.jqsrt.2007.10.010.
- A. A. Lacis and V. Oinas. A description of the correlated-k distribution method for modelling nongray gaseous absorption, thermal emission, and multiple scattering in vertically inhomogeneous atmospheres. *J. Geophys. Res.*, 96:9027–9064, May 1991.

- M. P. Lamb, W. E. Dietrich, S. M. Aciego, D. J. DePaolo, and M. Manga. Formation of Box Canyon, Idaho, by Megaflood: Implications for Seepage Erosion on Earth and Mars. *Science*, 320:1067–, May 2008. doi: 10.1126/science.1156630.
- H. Lammer, E. Chassefière, Ö. Karatekin, A. Morschhauser, P. B. Niles, O. Mousis, P. Odert, U. V. Möstl, D. Breuer, V. Dehant, M. Grott, H. Gröller, E. Hauber, and L. B. S. Pham. Outgassing History and Escape of the Martian Atmosphere and Water Inventory. *Space Science Rev.*, 174:113–154, January 2013. doi: 10.1007/s11214-012-9943-8.
- P. P. Lavvas, A. Coustenis, and I. M. Vardavas. Coupling photochemistry with haze formation in Titan’s atmosphere, Part I: Model description. *Planet. Space Science*, 56:27–66, January 2008a. doi: 10.1016/j.pss.2007.05.026.
- P. P. Lavvas, A. Coustenis, and I. M. Vardavas. Coupling photochemistry with haze formation in Titan’s atmosphere, Part II: Results and validation with Cassini/Huygens data. *Planet. Space Science*, 56:67–99, January 2008b. doi: 10.1016/j.pss.2007.05.027.
- S. Lebonnois, J. Burgalat, P. Rannou, and B. Charnay. Titan global climate model: A new 3-dimensional version of the IPSL Titan GCM. *Icarus*, 218:707–722, March 2012. doi: 10.1016/j.icarus.2011.11.032.
- M. C. Malin and M. H. Carr. Groundwater formation of martian valleys. *Nature*, 397: 589–591, February 1999. doi: 10.1038/17551.
- S. Manabe and R. T. Wetherald. Thermal Equilibrium of the Atmosphere with a Given Distribution of Relative Humidity. *J. Atmosph. Sciences*, 24:241–259, May 1967.
- M. Manga, A. Patel, J. Dufek, and E. S. Kite. Wet surface and dense atmosphere on early Mars suggested by the bomb sag at Home Plate, Mars. *Geophys. Res. Letters*, 39:L01202, January 2012. doi: 10.1029/2011GL050192.
- Mars Exploration Program Analysis Group. MEPAG (2005), Mars Scientific Goals, Objectives, Investigations, and Priorities. *white paper posted August, 2005 by the Mars Exploration Program Analysis Group at <http://mepag.jpl.nasa.gov/reports/index.html>*, page 31, August 2005.
- C. P. McKay and C. R. Stoker. The Early Environment and its Evolution on Mars: Implications for Life. *Reviews of Geophysics*, 27:189–214, 1989. doi: 10.1029/RG027i002p00189.
- C. P. McKay, J. B. Pollack, and R. Courtin. The thermal structure of Titan’s atmosphere. *Icarus*, 80:23–53, July 1989. doi: 10.1016/0019-1035(89)90160-7.
- M. A. Mischna, J. F. Kasting, A. Pavlov, and R. Freedman. Influence of carbon dioxide clouds on early martian climate. *Icarus*, 145:546–554, June 2000. doi: 10.1006/icar.2000.6380.

- M. A. Mischna, C. Lee, and M. Richardson. Development of a fast, accurate radiative transfer model for the Martian atmosphere, past and present. *Journal of Geophysical Research (Planets)*, 117:E10009, October 2012. doi: 10.1029/2012JE004110.
- M. A. Mischna, V. Baker, R. Milliken, M. Richardson, and C. Lee. Effects of obliquity and water vapor/trace gas greenhouses in the early martian climate. *Journal of Geophysical Research (Planets)*, 118:560–576, March 2013. doi: 10.1002/jgre.20054.
- T. D. Mitchell and P. D. Jones. An improved method of constructing a database of monthly climate observations and associated high-resolution grids. *Int. J. Climatology*, 25:693–712, May 2005. doi: 10.1002/joc.1181.
- J. M. Moore, A. D. Howard, W. E. Dietrich, and P. M. Schenk. Martian Layered Fluvial Deposits: Implications for Noachian Climate Scenarios. *Geophys. Res. Letters*, 30:2292, December 2003. doi: 10.1029/2003GL019002.
- S. R. Moore and D. W. G. Sears. On Laboratory Simulation and the Effect of Small Temperature Oscillations About the Freezing Point and Ice Formation on the Evaporation Rate of Water on Mars. *Astrobiology*, 6:644–650, August 2006. doi: 10.1089/ast.2006.6.644.
- C. E. Newman, C. Lee, Y. Lian, M. I. Richardson, and A. D. Toigo. Stratospheric superrotation in the TitanWRF model. *Icarus*, 213:636–654, June 2011. doi: 10.1016/j.icarus.2011.03.025.
- P. A. O’Gorman and T. Schneider. The Hydrological Cycle over a Wide Range of Climates Simulated with an Idealized GCM. *Journal of Climate*, 21:3815, 2008. doi: 10.1175/2007JCLI2065.1.
- W. Osterkamp and E. Hedman. Perennial-streamflow Characteristics Related to Channel Geometry and Sediment in the Missouri River Basin. *U.S.G.S. Prof. Paper*, 1242, 1982.
- M. Palucis, W. Dietrich, A. Hayes, R. Williams, S. Gupta, N. Mangold, H. Newsom, C. Hardgrove, F. Calef, and D. Sumner. The origin and evolution of the Peace Vallis fan system that drains to the Curiosity landing area, Gale Crater, Mars. *J. Geophys. Res. Planets*, 119:705–728, April 2014. doi: 10.1002/2013JE004583.
- J. T. Parrish. Climate of the Supercontinent Pangea. *Journal of Geology*, 101:215–233, March 1993. doi: 10.1086/648217.
- R. A. Parsons, J. M. Moore, and A. D. Howard. Evidence for a short period of hydrologic activity in Newton crater, Mars, near the Hesperian-Amazonian transition. *J. Geophys. Res. (Planets)*, 118:1082–1093, May 2013. doi: 10.1002/jgre.20088.
- A. A. Pavlov, J. F. Kasting, L. L. Brown, K. A. Rages, and R. Freedman. Greenhouse warming by CH₄ in the atmosphere of early Earth. *J. Geophys. Res.*, 105:11981–11990, May 2000. doi: 10.1029/1999JE001134.

- J. C. Penido, C. I. Fassett, and S. M. Som. Scaling relationships and concavity of small valley networks on Mars. *Planet. Space Science*, 75:105–116, January 2013. doi: 10.1016/j.pss.2012.09.009.
- J. T. Perron, J. X. Mitrovica, M. Manga, I. Matsuyama, and M. A. Richards. Evidence for an ancient martian ocean in the topography of deformed shorelines. *Nature*, 447: 840–843, June 2007. doi: 10.1038/nature05873.
- R. J. Phillips, M. T. Zuber, S. C. Solomon, M. P. Golombek, B. M. Jakosky, W. B. Banerdt, D. E. Smith, R. M. E. Williams, B. M. Hynek, O. Aharonson, and S. A. Hauck. Ancient Geodynamics and Global-Scale Hydrology on Mars. *Science*, 291: 2587–2591, March 2001. doi: 10.1126/science.1058701.
- R. Pierrehumbert and E. Gaidos. Hydrogen Greenhouse Planets Beyond the Habitable Zone. *Astrophys. J. Letters*, 734:L13, June 2011. doi: 10.1088/2041-8205/734/1/L13.
- R. T. Pierrehumbert and C. Erlick. On the Scattering Greenhouse Effect of CO₂ Ice Clouds. *J. Atmosph. Sciences*, 55:1897–1903, May 1998.
- J. B. Pollack, J. F. Kasting, S. M. Richardson, and K. Poliakov. The case for a wet, warm climate on early Mars. *Icarus*, 71:203–224, August 1987. doi: 10.1016/0019-1035(87)90147-3.
- S. E. Postawko and W. R. Kuhn. Effect of the greenhouse gases (CO₂, H₂O, SO₂) on Martian paleoclimate. *J. Geophys. Res.*, 91:431, March 1986. doi: 10.1029/JB091iB04p0D431.
- R. M. Ramirez, R. Kopparapu, M. E. Zugger, T. D. Robinson, R. Freedman, and J. F. Kasting. Warming early Mars with CO₂ and H₂. *Nature Geoscience*, 7:59–63, January 2014. doi: 10.1038/ngeo2000.
- N. O. Rennó, K. A. Emanuel, and P. H. Stone. Radiative-convective model with an explicit hydrologic cycle. 1. Formulation and sensitivity to model parameters. *J. Geophys. Res.*, 99:14429, July 1994. doi: 10.1029/94JD00020.
- L. S. Rothman, I. E. Gordon, A. Barbe, D. C. Benner, P. F. Bernath, M. Birk, V. Boudon, L. R. Brown, A. Campargue, J.-P. Champion, K. Chance, L. H. Coudert, V. Dana, V. M. Devi, S. Fally, J.-M. Flaud, R. R. Gamache, A. Goldman, D. Jacquemart, I. Kleiner, N. Lacome, W. J. Lafferty, J.-Y. Mandin, S. T. Massie, S. N. Mikhailenko, C. E. Miller, N. Moazzen-Ahmadi, O. V. Naumenko, A. V. Nikitin, J. Orphal, V. I. Perevalov, A. Perrin, A. Predoi-Cross, C. P. Rinsland, M. Rotger, M. Šimečková, M. A. H. Smith, K. Sung, S. A. Tashkun, J. Tennyson, R. A. Toth, A. C. Vandaele, and J. Vander Auwera. The HITRAN 2008 molecular spectroscopic database. *J. Quant. Spect. Rad. Trans.*, 110:533–572, June 2009. doi: 10.1016/j.jqsrt.2009.02.013.
- L. S. Rothman, I. E. Gordon, Y. Babikov, A. Barbe, D. Chris Benner, P. F. Bernath, M. Birk, L. Bizzocchi, V. Boudon, L. R. Brown, A. Campargue, K. Chance, E. A.

- Cohen, L. H. Coudert, V. M. Devi, B. J. Drouin, A. Fayt, J.-M. Flaud, R. R. Gamache, J. J. Harrison, J.-M. Hartmann, C. Hill, J. T. Hodges, D. Jacquemart, A. Jolly, J. Lamouroux, R. J. Le Roy, G. Li, D. A. Long, O. M. Lyulin, C. J. Mackie, S. T. Massie, S. Mikhailenko, H. S. P. Müller, O. V. Naumenko, A. V. Nikitin, J. Orphal, V. Perevalov, A. Perrin, E. R. Polovtseva, C. Richard, M. A. H. Smith, E. Starikova, K. Sung, S. Tashkun, J. Tennyson, G. C. Toon, V. G. Tyuterev, and G. Wagner. The HITRAN2012 molecular spectroscopic database. *J. Quant. Spect. Rad. Trans.*, 130:4–50, November 2013. doi: 10.1016/j.jqsrt.2013.07.002.
- K. E. Scanlon, J. W. Head, J.-B. Madeleine, R. D. Wordsworth, and F. Forget. Orographic precipitation in valley network headwaters: Constraints on the ancient Martian atmosphere. *Geophys. Res. Letters*, 40:4182–4187, August 2013. doi: 10.1002/grl.50687.
- D. W. G. Sears and S. R. Moore. On laboratory simulation and the evaporation rate of water on Mars. *Geophys. Res. Letters*, 32:L16202, August 2005. doi: 10.1029/2005GL023443.
- A. Segura, K. Krelow, J. F. Kasting, D. Sommerlatt, V. Meadows, D. Crisp, M. Cohen, and E. Mlawer. Ozone Concentrations and Ultraviolet Fluxes on Earth-Like Planets Around Other Stars. *Astrobiology*, 3:689–708, December 2003. doi: 10.1089/153110703322736024.
- T. L. Segura, O. B. Toon, and A. Colaprete. Modeling the environmental effects of moderate-sized impacts on Mars. *J. Geophys. Res.*, 113:E11007, November 2008. doi: 10.1029/2008JE003147.
- F. Selsis, D. Despois, and J.-P. Parisot. Signature of life on exoplanets: Can Darwin produce false positive detections? *Astron. Astrophys.*, 388:985–1003, June 2002. doi: 10.1051/0004-6361:20020527.
- D. E. Smith, M. T. Zuber, H. V. Frey, J. B. Garvin, J. W. Head, D. O. Muhleman, G. H. Pettengill, R. J. Phillips, S. C. Solomon, H. J. Zwally, W. B. Banerdt, T. C. Duxbury, M. P. Golombek, F. G. Lemoine, G. A. Neumann, D. D. Rowlands, O. Aharonson, P. G. Ford, A. B. Ivanov, C. L. Johnson, P. J. McGovern, J. B. Abshire, R. S. Afzal, and X. Sun. Mars Orbiter Laser Altimeter: Experiment summary after the first year of global mapping of Mars. *J. Geophys. Res.*, 106:23689–23722, October 2001. doi: 10.1029/2000JE001364.
- A. Soto. *Dynamical Paleoclimatology of Mars*. PhD thesis, California Institute of Technology, 2012.
- B. D. Stanley, M. M. Hirschmann, and A. C. Withers. CO₂ solubility in Martian basalts and Martian atmospheric evolution. *Geochimica Cosmochimica Acta*, 75: 5987–6003, October 2011. doi: 10.1016/j.gca.2011.07.027.
- D. J. Stevenson. Life-sustaining planets in interstellar space? *Nature*, 400:32, July 1999. doi: 10.1038/21811.

- F. Tian, J. F. Kasting, and S. C. Solomon. Thermal escape of carbon from the early Martian atmosphere. *Geophys. Res. Letters*, 36:2205, January 2009. doi: 10.1029/2008GL036513.
- F. Tian, M. W. Claire, J. D. Haqq-Misra, M. Smith, D. C. Crisp, D. Catling, K. Zahnle, and J. F. Kasting. Photochemical and climate consequences of sulfur outgassing on early Mars. *Earth Plan. Science Letters*, 295:412–418, July 2010. doi: 10.1016/j.epsl.2010.04.016.
- R. A. Urata and O. B. Toon. Simulations of the martian hydrologic cycle with a general circulation model: Implications for the ancient martian climate. *Icarus*, 226:229–250, September 2013. doi: 10.1016/j.icarus.2013.05.014.
- I. M. Vardavas and J. H. Carver. Solar and terrestrial parameterizations for radiative-convective models. *Planet. Space Science*, 32:1307–1325, October 1984. doi: 10.1016/0032-0633(84)90074-6.
- P. von Paris, J. L. Grenfell, H. Rauer, and J. W. Stock. N₂-associated surface warming on early Mars. *Planet. Space Science*, 82:149–154, July 2013a. doi: 10.1016/j.pss.2013.04.009.
- P. von Paris, F. Selsis, D. Kitzmann, and H. Rauer. The dependence of the ice-albedo feedback on atmospheric properties. *Astrobiology*, 13:899–909, October 2013b. doi: 10.1089/ast.2013.0993.
- R. Weingartner, G. Blöschl, D. Hanaah, D. Marks, J. Parajka, C. Pearson, M. Rogger, J. Salinas, E. Sauquet, R. Srikanthan, S. Thompson, and A. Viglione. Prediction of seasonal runoff in ungauged basins. In *Runoff Prediction in Ungauged Basins: Synthesis across Processes, Places, and Scales*, pages 102–134. Cambridge University Press, Cambridge, 2013.
- R. West, D. Crisp, and L. Chen. Mapping transformations for broadband atmospheric radiation calculations. *J. Quant. Spect. Rad. Trans.*, 43:191–199, March 1990.
- R. M. E. Williams, J. P. Grotzinger, W. E. Dietrich, S. Gupta, D. Y. Sumner, R. C. Wiens, N. Mangold, M. C. Malin, K. S. Edgett, S. Maurice, O. Forni, O. Gasnault, A. Ollila, H. E. Newsom, G. Dromart, M. C. Palucis, R. A. Yingst, R. B. Anderson, K. E. Herkenhoff, S. Le Moulic, W. Goetz, M. B. Madsen, A. Koefoed, J. K. Jensen, J. C. Bridges, S. P. Schwenzer, K. W. Lewis, K. M. Stack, D. Rubin, L. C. Kah, J. F. Bell, J. D. Farmer, R. Sullivan, T. Van Beek, D. L. Blaney, O. Pariser, R. G. Deen, and MSL Science Team. Martian fluvial conglomerates at gale crater. *Science*, 340(6136):1068–1072, 2013. doi: 10.1126/science.1237317.
- R. M. E. Williams, R. P. Irwin, D. M. Burr, T. Harrison, and P. McClelland. Variability in martian sinuous ridge form: Case study of Aeolis Serpens in the Aeolis Dorsa, Mars, and insight from the Mirackina paleoriver, South Australia. *Icarus*, 225:308–324, July 2013. doi: 10.1016/j.icarus.2013.03.016.
- W. J. Wiscombe and J. Evans. Exponential-sum fitting of radiative transmission functions. *J. Computational Physics*, 24:416–444, 1977.

- M. Woo. Permafrost hydrology in North America. *Atmosphere-Ocean*, 24:201–234, 1986. doi: 10.1080/07055900.1986.9649248.
- M. Woo. *Permafrost Hydrology*. Springer, Heidelberg, 2012.
- R. Wordsworth and R. Pierrehumbert. Hydrogen-Nitrogen Greenhouse Warming in Earth's Early Atmosphere. *Science*, 339:64–, January 2013. doi: 10.1126/science.1225759.
- R. Wordsworth, F. Forget, and V. Eymet. Infrared collision-induced and far-line absorption in dense CO₂ atmospheres. *Icarus*, 210:992–997, December 2010a. doi: 10.1016/j.icarus.2010.06.010.
- R. Wordsworth, F. Forget, F. Selsis, J. Madeleine, E. Millour, and V. Eymet. Is Gliese 581d habitable? Some constraints from radiative-convective climate modeling. *Astron. Astrophys.*, 522:A22, November 2010b. doi: 10.1051/0004-6361/201015053.
- R. Wordsworth, F. Forget, E. Millour, J. Head, J.-B. Madeleine, and B. Charnay. Global modelling of the early Martian climate under a denser CO₂ atmosphere: Water cycle and ice evolution. *Icarus*, 222(1):1–19, January 2013. doi: 10.1016/j.icarus.2012.09.036.
- R. D. Wordsworth, F. Forget, F. Selsis, E. Millour, B. Charnay, and J.-B. Madeleine. Gliese 581d is the First Discovered Terrestrial-mass Exoplanet in the Habitable Zone. *Astrophys. J. Letters*, 733:L48, June 2011. doi: 10.1088/2041-8205/733/2/L48.
- P. Xie and P. A. Arkin. Global Precipitation: A 17-Year Monthly Analysis Based on Gauge Observations, Satellite Estimates, and Numerical Model Outputs. *Bull. Amer. Meteor. Soc.*, 78:2539–2558, November 1997. doi: 10.1175/1520-0477(1997)078<2539:GPAYMA>2.0.CO;2.
- R. A. Yingst, L. C. Kah, M. Palucis, R. M. E. Williams, J. Garvin, J. C. Bridges, N. Bridges, R. G. Deen, J. Farmer, O. Gasnault, W. Goetz, V. E. Hamilton, V. Hipkin, J. K. Jensen, P. L. King, A. Koefoed, S. P. Le Mouélic, M. B. Madsen, N. Mangold, J. Martinez-Frias, S. Maurice, E. M. McCartney, H. Newsom, O. Pariser, V. H. Sautter, and R. C. Wiens. Characteristics of pebble- and cobble-sized clasts along the Curiosity rover traverse from Bradbury Landing to Rocknest. *J. Geophys. Res.*, 118:2361–2380, November 2013. doi: 10.1002/2013JE004435.
- Y. L. Yung, H. Nair, and M. F. Gerstell. NOTE: CO₂ Greenhouse in the Early Martian Atmosphere: SO₂ Inhibits Condensation. *Icarus*, 130:222–224, November 1997. doi: 10.1006/icar.1997.5808.